Inactivation of Stac3 Causes Skeletal Muscle Defects and Perinatal Death in Mice

Brad Michael Reinholt

Thesis submitted to the faculty of the Virginia Polytechnic Institute and State University
in partial fulfillment of the requirements for the degree of

Master of Science
In
Animal and Poultry Sciences

H. Jiang (Co-Chair)
D. E. Gerrard (Co-Chair)
A. L. Grant

January 27, 2012
Blacksburg, Virginia

Keywords: SH3 and cysteine rich domain 3 (Stac3), C1 domain, SH3 domain, myogenesis

Inactivation of Stac3 Causes Skeletal Muscle Defects and Perinatal Death in Mice

Brad Michael Reinholt

ABSTRACT

The Src homology 3 domain (SH3) and cysteine rich domain (C1) 3 (Stac3) gene is a novel gene copiously expressed in skeletal muscle. The objective of this research was to determine the role of Stac3 in development, specifically in skeletal muscle. We achieved this objective by evaluating the phenotypic effects of Stac3 gene inactivation on development in mice. At birth homozygous Stac3 null (Stac3-/-) mice died perinatally and remained in fetal position with limp limbs, but possessed otherwise normal organs based on gross and histological evaluations. The primary phenotypes displayed at term in Stac3-/- mice were reduced late gestational body weights, increased prevalence of myotubes with centrally located nuclei and severe deformities throughout all skeletal muscles. At embryonic day 18.5 (E18.5) Stac3-/- mice displayed a 12.7% reduction ($P < 0.001$) in weight compared to wild type (Stac3+/+) or heterozygous (Stac3+/-) littermates while at E15.5 body weights and morphology were similar. At birth (P0) and at E17.5, Stac3-/- mice had 59% and 24% ($P < 0.001$) more myotubes with centrally located nuclei, respectively, than Stac3+/- or Stac3+/+ littermates. Stac3-/- mice also displayed increased myotube and myofiber cross sectional area at P0 ($P < 0.001$) and E17.5 ($P < 0.05$) with disorganized fiber bundling. Overall, these data show Stac3 is necessary for development of viable offspring and suggest Stac3 plays a critical role in fetal development where its primary phenotype is exhibited in skeletal muscle.

ACKNOWLEDGEMENTS

A sincere appreciation is due my committee members for their guidance, patience and encouragement throughout this project. To Dr. Gerrard for the opportunity to conduct my graduate studies at Virginia Tech and providing me with challenges both academically and personally, Dr. Jiang for teaching me the importance diligence and techniques during my scientific research, and Dr. Grant for his valuable insight and support both present and past.

I would like to thank my lab mates, Xiaomei Ge, Jason and Tracy Scheffler, Suny Park, Eric England, Kim Fisher, Aihua Wang, Steve Kasten, Lidan Zhao, Ben Zhu and Greg van Eyk, who aided in multiple facets of this project. Especially to Xiaomei for the late nights, early mornings and long discussions during frustrating times. She was invaluable help as a research partner and as a friend. I also want to thank all of my fellow graduate students for their support and friendships that will continue long after Virginia Tech. I also appreciate technical support provided by Lee Johnson and Cathy Parsons.

I want to thank my friends and family for their continued love and support. Particularly to my best friend Angela Pavuk who always provided an ear to listen, encouragement, and an exuberant passion for life. My brother, father, and mother for their unconditional love, regardless of the circumstances I know my family and friends are there to support me. I also want to thank my past mentors who have helped shape the person I am. From them I learned work ethic, honesty, determination, appreciation for the processes of life, and to take chances. Also to learn from these experiences and apply that to my future endeavors. The support and values given by these people have provided me the self confidence and life tools I need to reach, and continue achieving my aspirations.

Table of contents

Page

Page

List of tables

Table Page

List of figures

Figure Page

CHAPTER I

Literature review

Introduction

Skeletal muscle is essential to human health and well-being and is at the core of the animal production industry. It is responsible for approximately 40 percent of body mass in mammals and provides support and locomotion (reviewed by Marieb and Hoehn, 2010; Pas et al., 2004). It is also a natural source of essential nutrients when consumed as meat (reviewed by Aberle, 2001). However, skeletal muscle formation is a complex process that is not fully understood. Thus, research is needed to identify important regulators in skeletal muscle development.

Skeletal muscle development is highly ordered. It follows a cascade of events that are chiefly regulated by a core set of gene transcription factors called the myogenic regulatory factors (MRFs). MRFs play important roles in activating muscle progenitor cells (MPCs) to become functional muscle fibers, or myofibers, by directing myogenic lineage (reviewed by Perry and Rudnicki, 2000). Myofibers are multinucleated cells created by the fusion of myoblasts. Myofibers are comprised of myofibrils of which the functional unit is the sarcomere. The sarcomere is responsible for contraction, or shortening of the myofiber. Within the sarcomere, myosin and actin proteins interact in unison to contract muscle when stimulated by motor neurons under voluntary control. These unique features of skeletal muscle permit its function to create locomotion and structural posture in animals.

In recent years skeletal muscle has received much attention because it can be induced to differentiate *in vitro,* thus making it an outstanding research model. Moreover, skeletal muscle possesses a unique stem cell population, called satellite cells, which have the ability to give rise to different cells (Kuang et al., 2007). This makes skeletal muscle an ideal tissue to research with clinical relevance in myopathies and other diseases.

Embryonic muscle development

Skeletal muscle development originates from somites, which are segmented blocks of the paraxial mesoderm that form in pairs, one on each side of the neural tube. Somites form in an anterior to posterior direction beginning at the most cranial end of the neural groove. As a result, the anteriorly located somites are more developed and have a more complex nervous system in the cervical and thoracic segments of the trunk compared to the lumbar or sacral segments. Initially the somites give rise to the sclerotome that forms the axial skeleton and then the dermomyotome. Subsequently, the dermomyotome further forms the myotome (skeletal muscle) and the dermatome (dermis) (Brand-Saberi and Christ, 2000). During somitogenesis, the paraxial mesoderm either becomes a somite or paraxial presomitic mesoderm (PSM). In this respect, the PSM is non-committed paraxial mesoderm. As somites form posteriorly, cells in the PSM migrate posteriorly hence extending the PSM (Christ and Ordahl, 1995). Somitogenesis can be broken down into three main components, segmentation, epithelialization, and specification.

Several new findings in the last decade have resulted in a better understanding of somitogenesis, specifically in the segmentation of the paraxial mesoderm. The latest research shows that somitogenesis depends on the somite segmentation clock which is a series of sequential molecular and cellular events (Aulehla and Herrmann, 2004). Oscillatory genes control the segmentation clock in a wave pattern (Palmeirim et al., 1997). Although there is a complex network of associated factors, the Wnt and Notch signaling pathways regulate this wave pattern by stimulating the initial stages of myogenesis. In turn, the targets of the Wnt-Notch pathways negatively regulate this pathway. This negative feedback loop forms a gradient of gene expressions that dictate the size and rate of somite formation. Also involved are fibroblast growth factors (FGFs). However, myogenesis cannot take place in the presence of certain FGFs,

specifically FGF8 expressed in the PSM. Therefore, FGF8 functions as a myogenesis inhibitor (Dubrulle et al., 2001; Dubrulle and Pourquie, 2004a, b). Activation of Wnt signaling in the neural tube activates transcription of the Notch transmembrane receptor proteins in the paraxial mesoderm through a poorly understood mechanism. Notch then becomes highly expressed in the region of the PSM that will form a somatic boundary. The Notch receptor binds Delta-like ligands, primarily Delta-like1 and Delta-like3. Binding of the Delta-like ligands perturbs FGF8 expression. The FGF8 inhibition allows expression of mesoderm posterior protein2 (Mesp2) and hairy1. Mesp2 and hairy1 act to induce Eph-A4 receptor expression in cells that will form the posterior end of the somite. The Eph-A4 receptor binds ephrin proteins, specifically ephrin B2. Ephrin proteins have repulsive properties and this repulsive property causes the cells in the PSM to separate from each other creating a fissure (reviewed by Dequeant and Pourquie, 2008). Therefore, expression of Notch and Mesp2 is primarily in cells most anterior of the somite and hairy1 and Ephrin B2 expression is primarily in cells most posterior of the somite. The receptor Eph-A4 is expressed in the cells most anterior of the PSM. This process repeats in waves segmenting the paraxial mesoderm. The number of somites depends on the rate of this segmentation process where in the mouse 65 pairs develop, but this process is accelerated as much as four-fold in some animals resulting as many as 500 pairs of somites in some snakes (reviewed by Gilbert, 2010).

As somites become segregated, the peripheral cells of the somite undergo epithelialization. Signals from the ectoderm cause a marked decrease in cell division control protein 42 homolog (Cdc42) expression levels in the peripheral cells of the somite. This alters the cytoskeleton of these epithelized cell creating a ‘box’ around the remaining mesenchymal cells of the somite which express higher levels of Cdc42 (Nakaya et al., 2004). The extracellular

matrix protein fibronectin and adhesion protein N-cadherin stabilizes epithelialization. Fibronectin functions with ephrin in boundary formation while N-cadherin adheres adjacent cells into an epithelium (Hatta et al., 1987; Lash et al., 1987; Linask et al., 1998). The epithelialization process is the first point where specialized cells are distinguishable within one individual somite, here epithelial cells and mesenchymal cells. Once epithelialization is complete, the somite begins expressing factors that segregate cells into distinct lineages.

The Hox gene family is responsible for polarity of the anterior-posterior axis and dictates specification. Although the Hox genes are active in early somitogenesis and specification of the somites as mesodermal cells is determined relatively early in development, it does not manifest an effect until after segmentation and epithelialization have occurred. In other words, Hox expression in the PSM dictates axis orientation and the effect of Hox on skeleton patterning seems to be already provided at the presomitic stage and not in the differentiating somites (Carapuco et al., 2005). In contrast, the commitment of cells within the somite to a specific myogenic lineage occurs later. Cells in the dorsal medial lip of the somite form primaxial muscles (back muscles) and are located most proximal to the neural tube. The cells in the ventral lateral lip of the somite form the abaxial muscles (or diaphragm, abdominal, and limb muscles) and are located most distal to the neural tube (Burke and Nowicki, 2003; Christ and Ordahl, 1995) (Figure 1). The boundary dividing the primaxial and abaxial myogenic precursor cells (MPCs) is the lateral somatic frontier (Christ and Ordahl, 1995). The somatic frontier is primarily attributed to factors such as Wnt, Sonic Hedgehog (Shh) or bone morphogenetic proteins (BMPs), and from where these factors are produced, the neural tube, notochord, or the lateral plate mesoderm. Wnt1 and Wnt3a from the dorsal region of the neural tube and Shh from the notochord induce the primaxial cells (Ikeya and Takada, 1998; Stern et al., 1995). At the

same time, Shh inhibits bone morphogenetic protein-4 (BMP4) in the primaxial region preventing induction of the MPCs from becoming limb or trunk muscles. Wnt proteins from the epidermis and BMP4 from the lateral plate mesoderm induce factors that denote the abaxial cells (the lateral plate mesoderm becomes the heart and circulatory system). This specifies their migration to the limb bud and ventral abdominal regions (Pourquie et al., 1996). The cells residing in the dorsal medial lip and ventral lateral lip of the somite are the first committed MPCs called myoblasts identified by the expression of MRFs, MyoD, and Myf-5. At this point myoblasts comprise the majority of the myotome (Figure 2). Myoblasts from the dorsal medial lip migrate to form the axial muscles and the myoblasts originating from the ventral lateral lip to the limb field that will form the limb bud and ventral abdominal muscles (Figure 3). Specific Hox gene expression in the posterior region of the limb bud and T-box (Tbx) gene expression recruit muscle progenitor cells from the ventral lateral lip to the limb field (reviewed by Gilbert, 2010).

Myoblasts from the dorsal medial lip migrate to form the axial muscles and the myoblasts originating from the ventral lateral lip to the limb field that will form the limb bud and ventral abdominal muscles (Figure 3). Specific Hox gene expression in the posterior region of the limb bud and T-box (Tbx) gene expression recruit muscle progenitor cells from the ventral lateral lip to the limb field (reviewed by Gilbert, 2010). The Tbx genes are specifically required for limb patterning where Tbx5 dictates the anterior segments directing forelimb formation and Tbx4 dictates the posterior segments directing hindlimb formation (Yonei-Tamura et al., 1999b). During migration to the limb bud, the myoblasts reduce MRF expression, but maintain high expression levels of the transcription factor Paired box-3 (Pax3). Pax3 controls the migration process of myoblasts to the limb bud by regulating c-met expression (also known as hepatocyte

growth factor receptor). Hepatocyte growth factor (HGH, also known as scatter factor) and its receptor, c-met, are crucial for the migration process. The importance of HGH and c-met was discovered when transgenic mice that had forced overexpression of HGH ectopically in the spinal cord developed skeletal muscle in the leptomeninges (membranes that surround the brain and the spinal cord) of the thoracic spinal cord region of mice (Takayama et al., 1996). A naturally occurring mutation of Pax3 in the DNA binding domain results in failed limb musculature formation (Epstein et al., 1994). Other factors such as retinoic acid production in the limb field stimulate FGFs (FGF7, and FGF10 among others) that are vital for proliferation of the limb bud and formation of overlapping ectodermal layers that becomes the apical ectodermal ridge (Stratford et al., 1996; Yonei-Tamura et al., 1999a). Once migration to the limb bud is complete, myoblasts increase MRF expression and myogenesis resumes.

Myoblasts continue to proliferate as long as they remain in the cell cycle. This is stimulated by the presence of growth factors, primarily FGF. Once these factors deplete and the myoblasts reach confluency they begin secreting fibronectin onto their extracellular matrix. Fibronectin binds to the α5β1 integrin receptor- the primary integrin receptor in myoblasts (Boettiger et al., 1995; Menko and Boettiger, 1987). This ultimately causes the myoblasts to align in a semi-organized row eventually forming myotubes. This alignment has been shown to be mediated by cadherins and cell adhesion molecules (CAMs) (reviewed by Knudsen, 1990). The complete fusion of myoblasts requires meltrins, which are homologous to fertilins. Fertilins are associated with sperm-egg fusion. Meltrin is up regulated in the myotome when myotube formation begins and meltrin inhibition blocks myoblast fusion. Meltrins are also important in muscle regeneration where they play a role in satellite cell fusion to existing fibers (Borneman et al., 2000; Yagami-Hiromasa et al., 1995). At the time of fusion, transcription of the MRF

myogenin and interlukin-4 (IL-4) is activated and the myoblasts withdraw from the cell cycle. Proliferating myoblasts withdraw from the cell cycle and become terminally differentiated myocytes expressing myogenin or MRF4. Myogenin initiates transcription of a host of muscle-specific genes and IL-4 recruits additional myoblasts that further promote differentiation and ultimately form multinucleated primary myotubes (Horsley et al., 2003). At this point, however, myotubes have limited functionality and contraction ability with the majority of their myogenic nuclei located in the center of the myotube. This is termed embryonic myogenesis. Subsequent waves of myogenesis must occur to form functional muscle fibers.

Muscle regulatory factors

Factors such as the Wnt and BMP proteins and their origin are vital in determining the lineage of mesodermal cells. However, these factors are paracrine factors that elicit a response in the MPCs. MPCs possess plasticity during development. MRFs induce commitment of MPCs to the myogenic lineage. MRFs are myogenic regulatory genes belonging to the MyoD family of transcription factors. The four core members are Myf-5, MyoD, MRF4, and myogenin (Braun et al., 1989; Davis et al., 1987; Rhodes and Konieczny, 1989; Wright et al., 1989). MRFs belong to the basic helix-loop-helix (bHLH) superfamily of transcription factors. Two main motifs found in the bHLH transcription factors allow them to bind to DNA and other proteins simultaneously. The basic domain found in bHLH transcription factors binds to specific DNA sequences called E-boxes, which in turn activate muscle-specific genes. The alpha-helical domain permits formation of homodimers or heterodimers with other proteins (Ellenberger et al., 1994; Ma et al., 1994; Murre et al., 1989). This allows members of the MRFs to work synergistically with other proteins to activate muscle specific genes in a distinct order. For example, MyoD interacts with a host of other proteins one of which is mitogen-activated protein kinase (p38) which then

facilitates binding of MyoD to myocyte enhancing factor-2 (MEF2). The MyoD-MEF2 heterodimer then initiates transcription of downstream muscle specific genes (Penn et al., 2004). Expression of MRFs are necessary for commitment of undifferentiated pluripotent cells into a myogenic lineage and for terminal differentiation into skeletal muscle. However, redundancy among the MRFs permits normal skeletal muscle development when one or more are inactivated.

Experiments creating homozygous double null mutations in Myf-5 and MyoD through gene knockout experiments resulted in complete absence of all skeletal muscle. Although the pups were born alive, they are motionless and die immediately. These mice fail to form myoblasts, and therefore are incapable of forming muscle fibers. Furthermore, no myogenin or MRF4 expression was detected in the double mutant which indicates MyoD and Mfy-5 lie genetically upstream in myogenesis (Rudnicki et al., 1993). However, when Myf-5 or MyoD are knocked-out individually skeletal muscle develops normally, although Myf-5 mutants die perinatally owing to incomplete formation of the distal ribs. Not only are mice homozygous null for MyoD completely viable and fertile, but Myf-5 expression is up regulated more than three-fold. When Myf-5 was knocked out there was no change in MyoD expression, but skeletal muscle developed (Braun et al., 1992; Rudnicki et al., 1992). These data denote the redundant function between MyoD and Myf-5 in commitment of MPCs to myoblasts. In the primaxial region of the somite (future back muscles), Wnt1 and Shh from the neural tube and notochord, respectively, initiate expression of Pax3 which in turn activates Myf-5 expression. In the abaxial region (future trunk muscles), Wnt-7a and BMP4 exposure activates Pax3 activate MyoD expression. Wnt and Shh must activate different pathways than do Wnt-7a and BMP4 causing different MRF expression patterns (Buckingham et al., 2006; Ordahl and Le Douarin, 1992). The specific regions within the somite dictate from where they receive signals and ultimately

determine future myogenic lineages (reviewed by Perry and Rudnicki, 2000). Altogether, Myf-5 and MyoD are responsible for the commitment of MPCs in two distinct locations in the myotome.

Myogenin and MRF4 play important roles in the differentiation and fusion of myoblasts into myotubes. Myogenin expression appears at the beginning of terminal differentiation in the formation of myocytes. Mice deficient in myogenin have severe muscle defects and die perinatally, but form a myoblast population capable of differentiation when cultured *in vitro* (Hasty et al., 1993; Nabeshima et al., 1993). Further investigation detected formation of primary muscle fibers, but not secondary muscle fibers (Venuti et al., 1995). Investigation of MRF4 (also known as herculin/Myf-6) revealed a surprising variation in its effect on myogenesis (reviewed by Weintraub, 1993). When MRF4 was deleted in mice, phenotypes ranged from complete viability of homozygotes to complete lethality. This variation is due to the close proximity of the Myf-5 and MRF4 coding regions on chromosome 10 and a cis-regulatory action on Myf-5. Alterations to the MRF4 coding region can effect Myf-5 expression. For example, the most severe MRF4 knockout allele expresses no Myf-5 RNA and is a developmental phenocopy of the Myf-5 null mutation causing severe rib abnormalities (Yoon et al., 1997). The MRF4 knockout increased myogenin expression as well (Zhang et al., 1995). Increased myogenin expression in these mutants indicated redundancy between myogenin and MRF4 in the differentiation of myoblasts into muscle fibers. Expression of MRF4 occurs in a wave-like pattern throughout muscle formation and maintenance most likely due to the cis-regulatory mechanism aforementioned. In the myotome, MRF4 is expressed during a brief time period in early myogenesis during cell proliferation; again, it is expressed in later stages of cell differentiation with peak expression in fully developed adult skeletal muscle (Patapoutian et al., 1995).

Together these data point to three overarching conclusions regarding the MRFs. First, they are necessary for the commitment of MPCs to a myogenic lineage. Second, they possess redundancy that evolutionarily protects myogenesis at the level of determination and differentiation. Finally, a certain threshold of MRF expression is required, illustrated by the up-regulation in some MRFs in the absence of others.

Important exogenous factors facilitate myogenesis and initiate proliferation and differentiation of myoblasts outside of the initial Wnt, Shh and BMP proteins. The positive effect of insulin-like growth factors (IGFs) on myogenesis is well known. *In vitro*, exogenous binding of IGF to its receptor stimulates proliferation, followed by increased differentiation. This effect on myogenesis is through activation of phosphatidylinositol 3-kinase (PI3-K), serine/threonine kinase (Akt, also known as protein kinase B) and mammalian target of rapamycin (mTOR) signaling pathways (Coolican et al., 1997; Kaliman et al., 1996). Meanwhile endogenously secreted IGF-II stimulates the expression of the cell cycle regulators p21 and myogenin. Through this autocrine regulatory mechanism myogenic differentiation and cell proliferation are both stimulated (Lawlor and Rotwein, 2000). However, the mechanism of this duel regulation of mutually exclusive events is poorly understood.

Fetal myogenesis

Generally, the embryonic period consists of organogenesis. The fetal period pertains to the continued growth and maturation of the developed organs and ends at birth. Skeletal muscle is no different in this regard. Once myoblasts have migrated to either axial (back) or limb regions, they fuse into multinucleated myotubes. The musculature system then undergoes hypertrophy to form functional muscle fibers. This proceeds in two waves, primary myogenesis, and secondary myogenesis. Primary myogenesis develops primary myotubes that begin

expressing myosin heavy chain (MyHC). Myosin heavy chain is an ATP-dependent motor protein with actin binding properties and is responsible for muscle contraction. Myosin is a large superfamily of proteins found throughout the animal and plant kingdoms consisting of at least 18 classes with multiple isoforms in each class. Their functions range from organelle trafficking in plant cells to muscle contraction in animals (Thompson and Langford, 2002). Class II is the type of myosin found in skeletal muscle. In skeletal muscle there are six main isoforms consisting of type I, type IIa, type IIb, type IIx(d), embryonic and fetal/perinatal. These fiber types draw on oxidative and glycolytic metabolisms. Type I is slow contracting utilizing oxidative metabolism. Type IIa maintains a primarily oxidative metabolism, but a fast contraction rate and more glycolytic capacity than type I. Type IIb draws primarily on glycolytic metabolism and is fast contracting. Type IIx fibers primarily draw on glycolytic metabolism, but also have oxidative capacity between that of type IIa and IIb, and are fast contracting isoforms (reviewed by Schiaffino and Reggiani, 2011). Embryonic MyHC is a slow type as well. The perinatal isofrom is more closely related to the two fast-type (IIb and IIx) MyHC isoforms (Periasamy et al., 1984). Even so, these properties are not absolute, but serve to justify the functional and phenotypical differences between fiber types in muscles.

Primary myotubes initially express MyHC type I along with embryonic and perinatal isoforms. These become scaffolds for which secondary myotubes form around. As the myotubes continue to develop, the nuclei migrate from the center of the myotube and relocate to the periphery of the fiber under the basal lamina forming primary fibers. Typically, these fibers maintain type I fiber properties, but can switch to type IIa. Secondary myotubes initially express type IIa, but not type I MyHC, embryonic or fetal. Secondary fibers also differ in their smaller diameter compared to primary myotubes. Secondary fibers can then give rise to type IIb and type

IIx(d), but typically not type I (Condon et al., 1990). Secondary myotubes, too, develop with centrally located nuclei, but these nuclei relocate to the periphery quickly, more so than primary myotubes. The mechanism of nuclear relocation that is responsible for myotube to myofiber shift is not well studied. Whether this is a passive process where the natural accumulation of muscle-specific proteins and contraction of the fiber push the nuclei toward the periphery, or if this is under a resolute mechanism is unknown.

Interestingly, these primary and secondary fibers develop from two distinct populations of myoblasts, one responsible for embryonic development, and a different population responsible for fetal development. These two populations develop sequentially during development and can be identified by expression of specific integrins and media requirements *in vivo* and *in vitro*. Early myoblasts found in limb muscle of a Day 12 embryo do not express α7 integrin and are able to differentiate in the presence of tetradecanoyl-phorbol 12 acetate (TPA). These comprise the embryonic population of myoblasts. The fetal population of myoblasts differs in their surface antigen and desmin expression, and in the sequence of the bHLH transcription factors and sarcomeric protein expression. Lending more support for different populations of myoblast, embryonic myoblasts are harvested at greater numbers in the embryonic stage, where as fetal myoblasts at collected at greater numbers in growing muscle (George-Weinstein et al., 1993; Stockdale, 1992). The concept of multiple populations of MPCs was challenged by Hughes and Blau (Hughes and Blau, 1992) when they labeled myoblasts and implanted them in postnatal rats. This allowed them to follow the myoblasts through adult myogenesis and they discovered that these myoblasts were able to fuse randomly with existing fibers showing no fiber type preference by the myoblasts. However, this was postnatal rather than embryonic or fetal development. Adult fibers have different gene expression patterns, cell signaling pathways, and

neural innervations that might alter the myoblast fusion. Myoblast environment contributes to gene expression it has now been shown that embryonic environment plays a critical role in activating these different populations of myoblasts (Buckingham et al., 2003).

The development of the neuromuscular junction is critical for muscle development, especially during secondary myogenesis. Duxson and Sheard (1995) demonstrated the points of innervation on primary fibers serves as a locus for secondary myofibers to develop. In the forelimb, primary fibers become innervated with nerves from the ventral rami whereas dorsal rami innervate the hindlimbs. The population of myoblasts that comprises the secondary fibers accrue around the point of innervation on the primary myofiber and then begin the process of alignment and fusion. Interestingly, myogenin expression has been shown to localize to the developing motor end-plate (reviewed by Rossant and Tam, 2002). Secondary myofibers continue to fuse to the cellular membrane of the primary myofibers creating a bundle of muscle fibers. This process continues until most myoblasts have fused and functional muscle fibers are developed.

A third population of cells exist called satellite cells (SCs) which reside just beneath the basal lamina juxtapose to the muscle fiber and are primarily responsible for adult myogenesis and muscle regeneration. They represent approximately 5% of the myonuclei present in adult muscle fibers (reviewed by Perry and Rudnicki, 2000). They are unique myogenic stem cells that possess mesenchymal plasticity to which gives them the ability to differentiate into different cell types such as adipocytes, and cells of the hematopoietic system (Csete et al., 2001; Endo, 2007; Jackson et al., 1999). These properties have spawned a great deal of research interest in the field of regenerative medicine. This research has generated several hypotheses about the origin of SCs. Recent investigations have revealed that SCs are derived from the central part of the

dermomyotome specifically between the primaxial and abaxial regions where a subpopulation of cells expresses both Pax3 and Pax7 (Gros et al., 2005; Kassar-Duchossoy et al., 2005; Relaix et al., 2005). It is believed this combination prevents the cells from undergoing myogenesis by preventing MyoD expression, but maintains their myogenic lineage for future activation (Buckingham et al., 2006) (Figures 2 and 3). This finding establishes the somite as the origin of all, embryonic, fetal and adult populations of MPCs.

When injury or disease occur, SCs activate through a mechanism that is still poorly understood. Whatever the case, SCs are a heterogeneous population of cells containing both stem- and muscle-like progenitor characteristics. In recent experiments, adult SCs expressing Pax7, but not Myf-5 were capable of asynchronous division into two types of cells: a Pax7 and Myf-5 positive cell and a Pax7 positive Myf-5 negative cell. The former differentiates into muscle while the latter returns to the stem cell population. Discovery of this dynamic property has opened the discussion for SCs as potential in therapeutic applications (Kuang et al., 2007).

Mouse development

Mice are valuable models for studying muscle development, though the specific developmental timeline in the mouse compared to other mammals is clearly different. Although somitogenesis is a highly conserved process among vertebrates, the chronology of specific events has greater variation. Recall, mice give birth to pups at approximately 20 days *post coitum* or embryonic day 20 (E20) (19.27 ± 0.042 in the C57BL/6J strain used in this study) (Murray et al., 2010). In the mouse, by E8 eight somites have developed. In contrast, it may take up to 21 days for eight somites to appear in developing bovine embryos, while the gestation length is approximately 284 days *post coitum* (reviewed by McGeady, 2006). The sequences of events in mice are more rapid than in other mammals (e.g. cattle), which may largely be due to animal

size. Therefore, this also allows less time for growth compared to other mammals resulting in a less developed young animal. For example, mice are born with their eyes closed and without the ability to balance themselves to walk. Meanwhile a newborn calf can stand and walk within minutes after birth.

Specifically in mice, at E7.5 the first somites appear. Within 24 hours up to eight somites develop. *In situ* hybridization studies discovered the first Mfy-5 transcripts by E8. By E9.75 myoblasts can be distinguished in the dermomyotome by MyoD and Myf-5 expression in the primaxial and abaxial regions, respectively. At E9 to E11.5, there is also transient expression of MRF4. However, whether MRF4 has a function at this early embryonic stage, or is merely a consequence of the close proximity of the MRF4 and the Myf-5 coding regions remains unknown. MyoD and Myf-5 reduce expression in MPCs in preparation for migration into the limb bud. Between E9.25 and E10.5 all cells that are destine to migrate to the limb bud, or axial muscles, have completed their migration. By E10.5, expression of MyoD and Myf-5 resumes and, therefore, so does myogenesis. By E11, the myoblasts begin expressing myogenin and embryonic MyHC along with resumed expression of MRF4. For proper terminology, when myoblasts express the differentiation factor myogenin or MRF4 they are considered myocytes which then fuse to form myotubes. By E13, the myocytes begin alignment and fusion and the first multinucleated myotubes appear. By E13.5, somitogenesis is complete and 65 pairs of somites have developed. Between E12 and E16, MRF4 expression is reduced, even though myotube formation continues during this period. On E16, secondary myofibers begin forming around the primaries. After E16, not only does MRF4 increase expression to coincide with secondary myogenesis, but from that point through the life of the animal MRF4 has the highest expression pattern among the MRFs (reviewed by Rossant and Tam, 2002). Muscle fibers

continue hypertrophy from E16 through maturity. As somitogenesis, myogenesis arises in an anterior to posterior manner as well. Expression of MRFs first appear in the forelimb and then in the hindlimb. More precisely, myogenin transcripts are detected in the forelimb at E11 and subsequently in the hindlimb at E11.5. At any rate, the overall expression pattern in the mouse exemplifies the distinct and ordered mechanism of embryonic, fetal, and adult myogenesis (Figure 4).

Because little evidence exists for new muscle formation after fetal development, or birth, the number of muscle fibers is entirely dependent on the proliferation of the myoblasts prior to differentiation. Parameters limiting the proliferation rate or total abundance of myoblasts severely limit muscle size in adulthood. A difference in size is found across species and is primarily attributed to the number of muscle cells. Therefore, the difference between the biceps femoris in a mouse differs from that of a pig only in the number of muscle cells originally produced. Again, pointing to the importance of proliferation regulation in the early stages of development.

The Src homology three and cysteine rich domain gene family

The Src homology three and cysteine rich domain (Stac) gene family consists of three members, Stac, Stac2 and Stac3 which are encoded by chromosomes 9, 11, 10, respectively in mice (Kawai et al., 1998). Stac proteins contain two well-recognized motifs; a Src homology three (SH3) domain and a cysteine rich (C1) domain. Suzuki et al (1996) first reported the discovery of Stac and was the first protein discovered that consisted of only a SH3 and C1 domain in a single peptide (Figure 5). They also determined that Stac expression begins at E13.5 and continues through adulthood with peak intensity approximately ten days after birth, or P10, in neurons. Furthermore, they discovered Stac protein was predominantly located in the

cytoplasm rather than the nucleus or in association with the membrane. These results supported the hypothesis that the Stac proteins normally reside in soluble form in the cellular cytosol fraction (Suzuki et al., 1996). The two motifs found in this family of proteins are both characteristic of proteins associated with second messenger signal transduction cascades. Neither possesses kinase activity alone, but modulate several kinase pathways (Abrams and Zhao, 1995; Colon-Gonzalez and Kazanietz, 2006; Stahl et al., 1988). These structural motifs combined with the fact that the Stac proteins do not possess any catalytic domains support a hypothesis that they might act as adaptor proteins in cell signaling pathways.

Initially discovered in the Src family of protein kinases, the SH3 domain is a prevalent protein–protein interaction motif. The SH3 domain is a 60 amino acid sequence that binds proline rich regions featuring a consensus sequence of -X-P-p-X-P-, specifically at the nitrogen backbone (Nguyen et al., 2000). This consensus sequence is present in numerous other protein families such as, Crk, Phospholipase C and myosins (Geli et al., 2000; Goodson et al., 1996; Mayer et al., 1988; Stahl et al., 1988). However, in adapter proteins involved in signal transduction such as Grb2, SH3 domains are typically accompanied by SH2 domains. These proteins receive signals through interaction of SH2 domains with specified phosphotyrosine residues in other receptor proteins and transfer the signal to the target proteins through SH3 domains (Schlessinger, 1994). Still, the Stac proteins do not contain a SH2 domain and therefore must have a different mechanism of action.

The C1 domain is an approximately 50 amino acid sequence that primarily binds the membrane bound second messenger diacyglycerol (DAG), and phorbol esters (Kazanietz et al., 1995a; Ono et al., 1989). The C1 domain found in the Stac family is atypical based on amino acid sequence. Some other proteins that contain atypical C1 domains are c-raf and PKCι among

others (Colon-Gonzalez and Kazanietz, 2006). An atypical C1 domain is the result of non-cysteine amino acid changes causing structural modifications that inhibit ligand binding, but not the overall folding of the protein (Kazanietz et al., 1994). Although not resolute as some atypical C1 domains can still bind DAG, this atypical C1 domain makes it possible that this specific protein family does not directly bind DAG or phorbol esters. In fact, Suzuki et al. (1996) demonstrated that a C1 fusion protein to Stac did not show any activity in phorbol ester binding. However, the atypical C1 domain has been shown to interact with G-protein coupled receptors (Brtva et al., 1995). Therefore, the Stac protein family might act in a G-protein coupled receptor pathway. Regardless, it appears that the C1 domain in the Stac protein family could bind with a membrane bound second messenger or cytosolic signal transduction protein, or proteins, of some kind.

The three Stac members are heterogeneously expressed among tissues. The first two members, Stac and Stac2, are expressed specifically in neurons. They are mutually exclusive markers for nociceptive peptidergic neurons and nonpeptidergic neurons, respectively, in the dorsal root ganglia neurons (Legha et al., 2010). To date, no published research has proposed a possible biological function for Stac or Stac2 in nervous tissue, only the location of the transcripts. The third member, Stac3, has an expression pattern that differs a greatly from Stac and Stac2. Expression of Stac3 is almost exclusively in skeletal muscle (Ge, 2012). Still, no data regarding Stac3 and its potential function in skeletal muscle exists. We conclude that given the high expression pattern of Stac3 in skeletal muscle, it could have a significant role in proliferation, fusion, or differentiation of skeletal muscle.

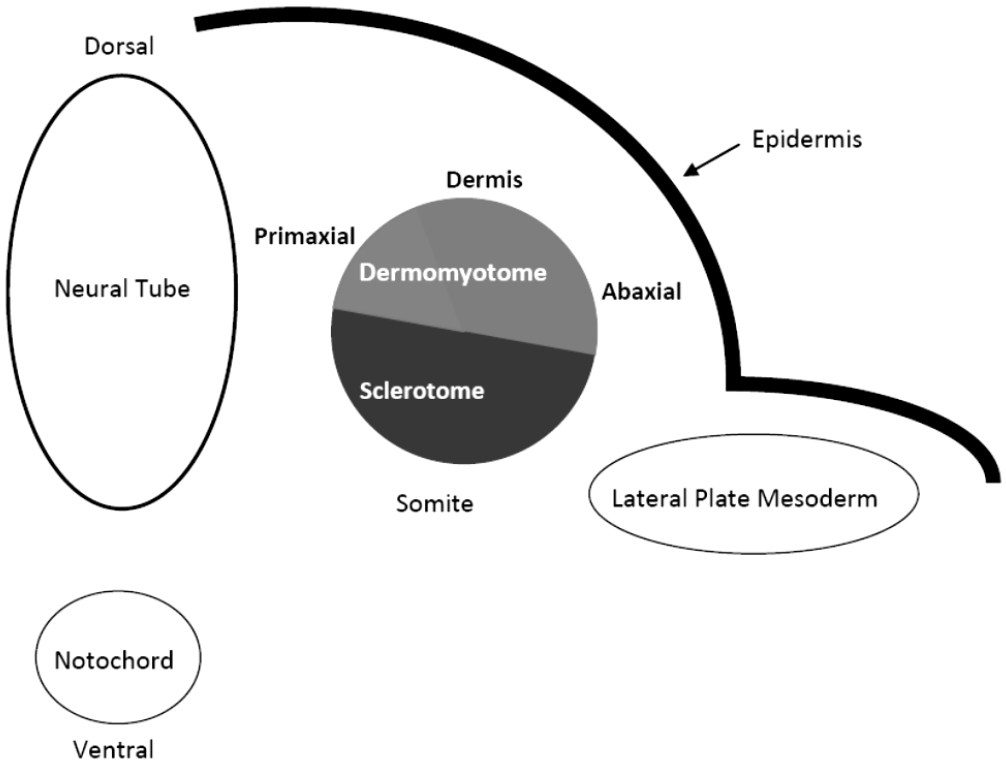

Figure 1. Diagram illustrating the segregation of the sclerotome and dermomyotome. The dermomyotome is comprised of the future myotome and dermatome. The myotome can then be subdivided into the primaxial and abaxial regions of the somite. The primaxial region is responsible for the formation of the back muscles and the abaxial region is responsible for the formation of the abdominal and limb muscles (adapted from Gilbert et al., 2010).

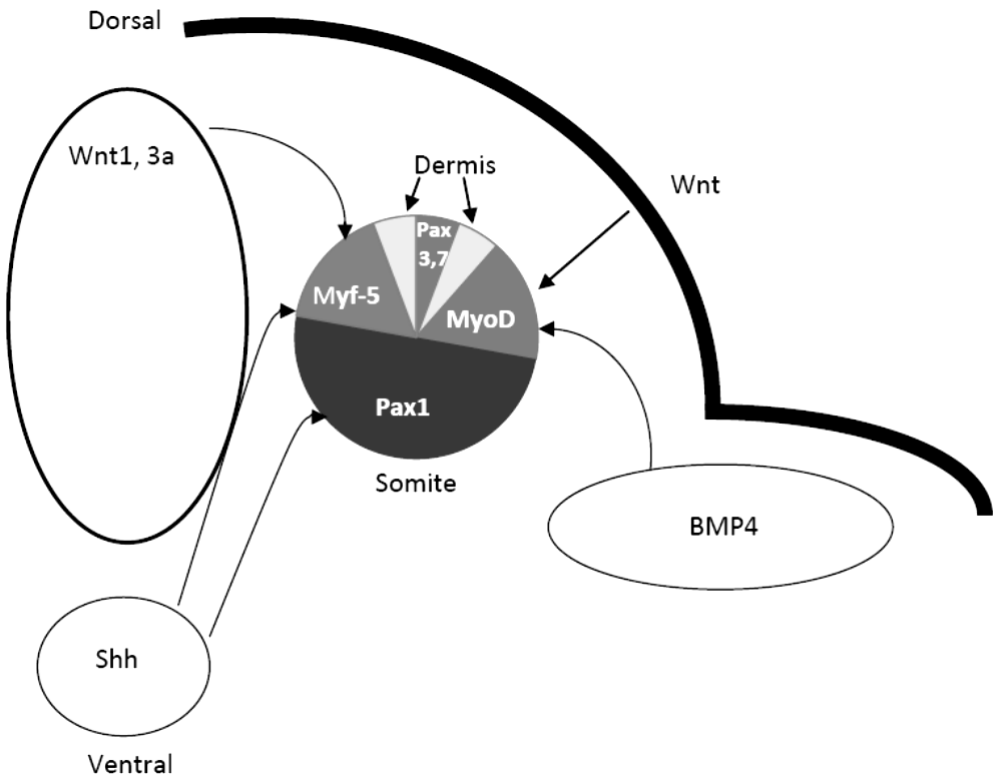

Figure 2. Diagram illustrating the expression pattern of myogenic regulatory factors and other transcription factors in the somite during myogenic determination. Factors from the dorsal neural tube, notochord and epidermis determine expression pattern of myogenic transcription factors in the somite (adapted from Gilbert et al., 2010).

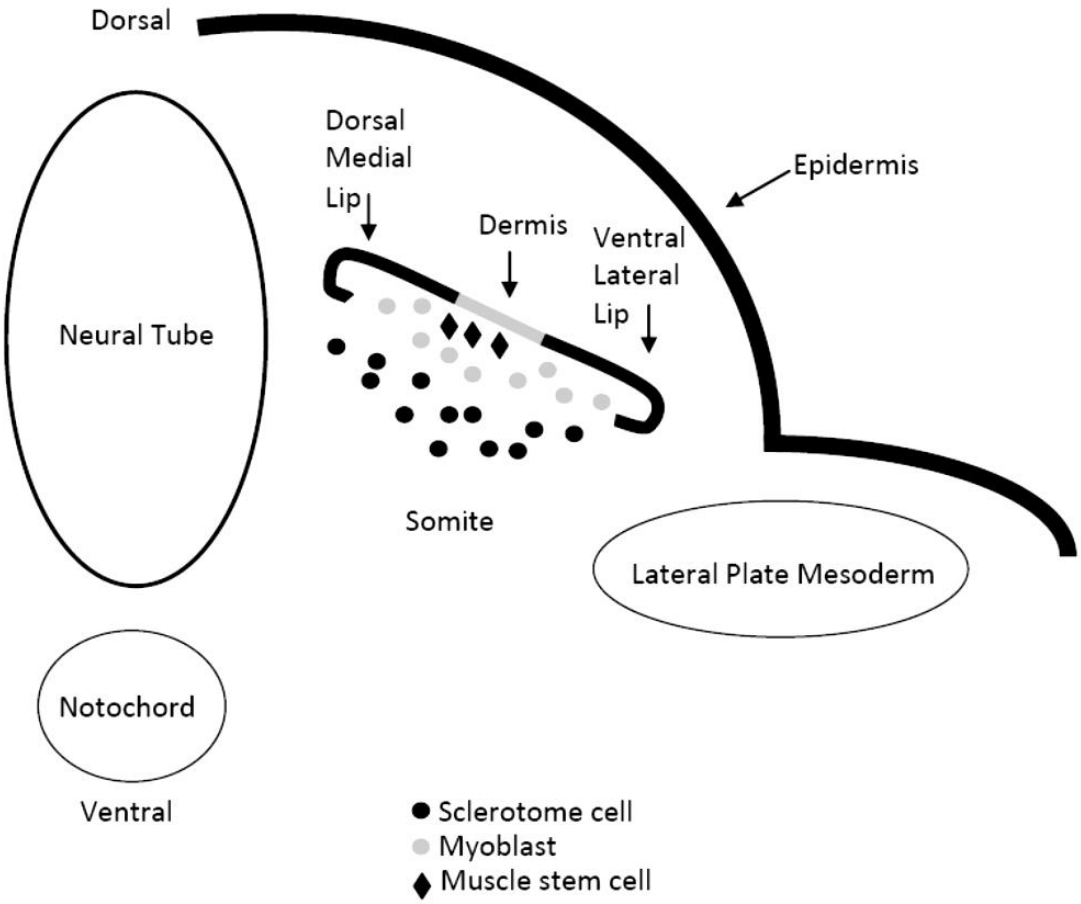

Figure 3. Myoblasts migrate from the dorsal medial lip to form the axial muscles and the myoblasts from the ventral lateral lip to form the abdominal and limb muscles. Muscle stem cells (satellite cells) originating from the dermis are present and expressing both Pax3 and Pax7 in the somite (adapted from Gilbert et al., 2010).

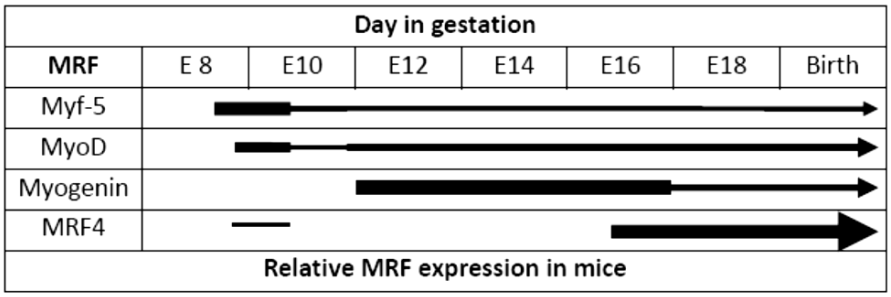

Figure 4. Diagram showing the timeline expression of myogenic regulatory factors (MRFs) in the developing mouse. The girth of the arrow indicates relative level of expression of each MRF. Importance of certain time points are emphasized by significant overlaps in MRF expression.

1 MTEKEVVESP QPPFPGETPQ SGLQRLKQLF KKGSPETAEM EPPPEPQANG EAVGAGGGPI
61 YYIYEEEEEE EEEEEPPPEP PKLVNDKPHK FKDHFFKKPK F**C**DV**C**ARMIV LNNKFGLR**C**K
121 N**C**KTNIHEH**C** QSYVEMQR**C**F GKIPPGFRRA YSSPLYSDQQ YAVSAANRND PVFETLRVGV
181 IMANKERKKG QADKKNPLAA MMEEEPESAR PEEGKSQDGN NAEKDKKAEK KTPDDKNKQP
241 GFQQSHYF***VA LYRFKALEKD DLDFPPGEKI TVIDDSNEEW WRGKIGEKVG FFPPNFIIRV***
301 RAGERVHRVT RSFVGNREIG QITLKKDQIV VQKGDEAGGY VKVYTGRKVG LFPTDFLEEI

Figure 5. Amino acid sequence of Stac3 *(mus musculus*) (NM_177707). The cysteine rich (C1) domain is highlighted in gray with the cysteine residues in bold script. The Src homology 3 domain is highlighted in bold and italicized script. In Stac3 the atypical C1 domain is determined by changes in non-cysteine amino acids, specifically at positions 22-25 and 27, of the C1 domain.

CHAPTE II.

Inactivation of Stac3 causes skeletal muscle defects and perinatal death in mice

Introduction

Src homology three and cysteine rich domain (Stac) was first discovered as a neuron specific protein with expression beginning at embryonic day 13.5 and continuing through adulthood with peak expression at day 10 after birth. Stac was found to have an amino acid sequence consisting of a Src homology three (SH3) domain and a cysteine rich (C1) domain (Suzuki et al., 1996). Since the initial discovery of Stac, two more members have been discovered in the Stac protein family, Stac2 and Stac3 (Legha et al., 2010). The SH3 and C1 domains are implicated in numerous intracellular signal-transducing pathways, although neither possesses catalytic activity directly (Abrams and Zhao, 1995; Colon-Gonzalez and Kazanietz, 2006; Stahl et al., 1988).The SH3 domain facilitates protein–protein binding at proline rich sequences, specifically at the nitrogen backbone (Nguyen et al., 2000). This sequence is present in many protein families such as Crk, Phospholipase C, and myosins (Geli et al., 2000; Goodson et al., 1996; Mayer et al., 1988; Stahl et al., 1988). However, in adapter proteins involved in signal transduction such as Grb2, SH3 domains are typically accompanied by SH2 domains (Schlessinger, 1994). The C1 domain binds the membrane bound second messenger diacylglycerol and is found in the protein kinase C protein family among others. Specifically, the Stac family possesses an atypical C1 domain. The atypical C1 domain is characterized by non-cysteine amino acid changes within the cysteine rich domain. Some proteins containing atypical C1 domains are c-raf and PKCι among others (Colon-Gonzalez and Kazanietz, 2006). Although these domains are well characterized, the specific function or mechanism of the Stac protein family is unknown, but these structural motifs suggest they work in signal transduction pathways.

Stac and Stac2 have been found to be exclusively expressed in a population of neurons in the dorsal root ganglia, specifically nociceptive peptidergic neurons and nonpeptidergic neurons, respectively (Legha et al., 2010). Stac3, however, is primarily expressed in skeletal muscle (Ge, 2012), suggesting that it might have unique functions in skeletal muscle.

Skeletal muscle fibers are syncytia that develop from mononulceated myogenic cells, or myoblasts. Myogenic precursor cells become activated giving rise to proliferating myoblasts. In response to extracellular cues, myoblasts withdraw from the cell cycle and fuse to form multinucleated myotubes (reviewed by Perry and Rudnicki, 2000). Myotubes mature into primary fibers which subpopulations of myoblasts use as a scaffold for fusion and secondary fiber formation. This process occurs in two waves called primary and secondary myogenesis during late embryonic and fetal development. Postnatal muscle growth is primarily attributed to hypertrophy of the muscle fibers whereas muscle stem cells, or satellite cells, are responsible for postnatal myogenesis (reviewed by Brand-Saberi, 2002). Each phase is complex series of orchestrated events that are not fully understood. Given the importance of skeletal muscle to human health and well-being, and its economic relevance to agriculture, additional research is needed to identify important regulators in skeletal muscle development. Considering the high expression pattern of Stac3 in skeletal muscle, we hypothesize it has a fundamental role in skeletal muscle growth, development or regeneration. We tested this hypothesis by evaluating the phenotypic effects of Stac3 gene deletion on skeletal muscle development in mice.

Materials and methods

Animals and design

The Virginia Tech Institutional Animal Care and Use Committee approved all protocols and procedures involving animals for this study. Mice heterozygous for the Stac3 allele (+/-) on a C57BL/6J background were obtained from the Knockout Mouse Project (KOMP; University of California at Davis) (Collins et al., 2007). Male and female Stac3+/- mice developed by using a trapping method of gene targeting were mated to produce Stac3-/- offspring (see Appendix A). To determine the day in gestation, visual observation of a vaginal plug in the morning was considered embryonic day 0.5 (E0.5) *post coitum*. Genotypes were determined by PCR on genomic DNA isolated from ear notches using two different primer sets. Primer set 1 flanked the third loxP site amplifying the insertion in the Stac3-/- (344 bp product) or the Stac3+/+ sequence (317 bp product) (Figure 6). Primer set 2 flanked the entire gene trap insertion resulting in a product too large to be amplified under our experimental conditions (> 1000 bp) or the Stac3+/+ sequence (468 bp product) (Figure 7). Primer sequences: Set 1: forward 5′-CTCCATAGCTCTACCGCAGTC-3′ reverse 3′-CTCTGCCTTGTGAGTGTGGA-5′. Set 2: Forward 5′-TGTTGGGCTTCTTCGTCTCT-3′ Reverse 3′-TGGTACCTTGTGTGGTGGTG-5′. The PCR conditions were 35 cycles of 94° C for 30 sec, 60° C for 30 sec, 72° C for 1 min.

Growth performance

Body weights of fetuses *in utero* were collected immediately after removal from the euthanized female. Postnatal growth performance was measured weekly from mice three weeks of age until six weeks. Physiologically this is approximately the time from weaning until sexual maturity.

Tissue collection, fixation, and sectioning

Mice were collected immediately after parturition or by dissection of full term pregnant females. Control offspring (P0) were euthanized with carbon dioxide and cervical dislocation. Body cavities were exposed to facilitate uniform fixation throughout the tissues by severing the skin on both the dorsal and ventral side of the midline. Mice were fixed for approximately 48 h in 10% neutral buffered formalin then placed in Tissue Bath Cassettes IV (aqua) (Thermo Fisher Scientific Waltham, MA) and a 70% alcohol solution until processing (see Appendix B). Hind limbs were carefully removed at the knee and embedded in paraffin, then sectioned on a Thermo Scientific HM 340E rotary microtome (Thermo Fisher Scientific Waltham, MA). Once distinguishing features of the lower leg (or *crus*) were observed, three serial 6 μm thick sections approximately 60 - 100 μm apart were collected until representative sections from the widest girth of the lower leg were captured. Sections were then mounted on Superfrost® Plus micro slides (VWR Radnor, PA) (see Appendix C). Sections were deparaffinized using xylene and rehydrated through graded alcohol solutions of 100%, 95%, 80% and 70% (see Appendix D).

Immunohistochemistry

For analysis, slides were stained with hematoxylin and eosin (H&E) or Immunohistochemistry (IHC) was performed. For H&E staining, standard protocols were utilized (see Appendix E). For IHC, heat-induced antigen retrieval was performed first to remove cross-linking caused by the fixative. Briefly, slides were boiled in 10 mM citrate buffer adjusted to pH 6 at approximately 95º C for 30 min. Slides were allowed to cool for 20 min and then washed in PBST (PBS with 0.05% Tween-20) for 2 min twice on a shaker (see Appendix G). Nonspecific binding was blocked with 5% goat serum **(**Sigma-Aldrich, St Louis, MO) (or serum from host of preferred secondary antibody) diluted in PBS for 1 h at room temperature. Primary

antibodies were diluted in 5% goat serum applied to the slide and incubated overnight at 4º C. The following primary antibodies used: all sarcomeric myosin heavy chain (MF20, 1:200, Developmental Studies Hybridoma Bank, Department of Biology, University of Iowa, Iowa City, IA), Myogenin (F5D, 1:100, Developmental Studies Hybridoma Bank, University of Iowa, Iowa City, IA) and MyoD1 (M-318, 1:100, Santa Cruz Biotechnology, Santa Cruz, CA). Slides were then washed 3 times for 5 min each in PBS under agitation, and incubated with an appropriate secondary antibody diluted in 5% goat serum. Secondary antibody used was DyLight® 594-conjugated goat anti-mouse (DyLight® 594, 1:200, Thermo Scientific, Rockford, IL). Cell membranes were stained with Lectin (Wheat Germ Agglutinin, 1:400, Invitrogen, Carlsbad, CA) and nuclei were counter stained (DAPI) using the secondary antibody dilution. Secondary antibodies were incubated for 1 h at room temperature. Slides were washed 3 times for 5 min each in PBS on a shaker. Aqueous Prolong® Gold antifade reagent (Invitrogen, Carlsbad, CA) mounting medium was added and 22 x 50 mm x 1.5 thickness (0.18 mm) cover slips (Thermo Fisher Scientific Waltham, MA) were applied over the sections (see Appendix H).

Histological imaging

Immunohistchemistry was visualized using fluorescent microscopy. Fluorescent images were captured with a Nikon eclipse E600 microscope connected to a QColor3 digital camera (QImaging, Surrey, British Columbia, Canada) using the Q-Capture suite software program (Olympus America Inc., Center Valley, PA) or a Nikon eclipse TS100 (Eclipse Ti microscope system) (Nikon Imaging Inc. Melville, NY) connected to a CoolSNAP HQ2 monochrome camera (Photometrics, Tucson, AZ) using a NIS-Elements AR Ver3.1 software program (Nikon Imaging Inc. Melville, NY). Light microscopy images were captured using a Nikon eclipse E600

microscope connected to a QColor3 digital camera using the Q-Capture suite software program at 4X, 10X or 20X magnification.

Muscle fiber characteristics

The *extensor digitorum longus* (EDL) was used to determine muscle fiber characteristics due to its uniformity, ease of muscle identification and recognized acceptance in research applications. Nuclear density and myotube percentage were measured using Image-Pro Plus Version 6.2 software program (Media Cybernetics, Silver Spring, MD). Data were subsequently transferred into an Excel spreadsheet (Microsoft Office, 2007). Myotube percentage was defined as the number of myosin heavy chain positive and centrally nucleated myotubes or myotubes with an open core ≥ 1 μm in diameter. Myotubes with a centrally located nuclei and myotubes with an open core were counted separately and combined, then divided by the combined total of myofibers and myotubes. For calculations a grid containing twelve- 5 mm^2 boxes was used on each section analyzed. Of these, five boxes were randomly selected where all myofibers and myotubes were counted. A minimum of 150 myofibers and myotubes were counted per individual.

Myonuclear density was determined by counting the number of myonuclei in direct contact with or in the center of a myofiber or myotube. Number of nuclei per 50 μm of a myofiber on H&E stained sagittal limb sections of the EDL were used. A minimum of sixteen fibers per animal from random locations were included in this counting.

Total myofiber number and average cross sectional areas (CSA) of myofibers were measured using the NIS-Elements AR Ver3.1 software (refer to *Histological imaging***)**. Total fiber number was determined by counting and averaging all myosin heavy chain positive fibers on three serial cross sections at the widest girth of the EDL muscle. To determine the widest

girth of the EDL, serial sections were stained with H&E until the largest CSA of the EDL was confirmed. Mean cross sectional area was calculated from a minimum of 150 randomly selected myosin heavy chain positive myofibers per animal. To be included in this CSA analysis, the myofiber must have had a distinguishable membrane on the cross sections and be positive for MyHC (see *Immunohistochemistry*).

Reverse Transcription (RT) –PCR

Tissue samples collected for knockout confirmation from E17.5 fetuses were brain, heart, intestine, kidney, liver, lung, tongue and skeletal muscle from all four limbs (Figure 8). Samples were flash frozen in liquid nitrogen. Total RNA was isolated with an RNeasy® Mini Kit following the manufacturer's animal tissue protocol (Qiagen, Valencia, CA.). Purity and quantity of RNA was determined using a NanoDrop 2000 Spectrophotometer (Thermo Scientific, Wilmington, DE). cDNA was transcribed from total RNA using 1.0 ng/µl RNA mixed with 4.0 µl 5x reaction buffer (M298 ImProm-II™) (Promega, Maddison, WI), 0.5 µl Ribonuclease inhibitor (N251A rRnasin®) (Promega), 1.0 µl Reverse transcriptase (M314A ImProm-II™) (Promega), 4.8 µl MgCl2 (Promega) and nuclease-free H_2O (Promega) to a final volume of 15.0 µl. The Stac3 sequence was amplified using the following PCR primer sequences: forward 5′-TACAGCGACCAACAGTACGC-3′and reverse 5′-TCTGCATTGTTTCCATCCTG-3′. Briefly master mix and RNA was incubated at 25º C for 5 min, then 42º C for 1 h followed by 70º C for 15 min on a PCR machine. An Eppendorf Mastercycler gradient (Hamburg, Germany) PCR machine was used where the template was amplified for 30 cycles. The PCR products were electrophoresed on a 2% agarose gel for 45 min at 110 V, visualized by ethidium bromide staining and imaged with FluorChem™ SP imaging system (Alpha Innotech, Johannesburg, South Africa).

Transmission Electron Microscopy

Transmission Electron Microscopy (TEM) was used to evaluate the ultra structure of the EDL muscle. All TEM was performed by the morphology service laboratory of the Virginia-Maryland Regional College of Veterinary Medicine. Briefly, lower leg samples were fixed in 3% glutaraldehyde diluted in PBS. In a fume hood, samples were trimmed to fit the mold and washed twice in 0.1 M Na cacodylate buffer (or appropriate buffer) for 15 min. Samples were then post-fixed in 1% OsO_4 in 0.1.M Na cacodylate buffer for 1 h, and then washed twice for 10 min in 0.1 M Na cacodylate. Samples were then dehydrated in graded ethanol solutions increasing in concentration as follows: 15%, 30%, 50%, 70%, 95%, 100%, and lastly submerged in propylene oxide allowing 15 min in each solution. Samples were then infiltrated with a 50:50 solution of propylene oxide:Poly/Bed 812 for 6-24 h completing infiltration with 100% mixture of Poly/Bed 812 for 6 - 12 h. Samples were then embedded in fresh 100% Poly Bed 812 resin molds. Molds were placed in a 60^{o} C oven for at least 48 h to cure. After embedding, thin sections (60 - 90 nm) were cut. Sections were stained with uranyl acetate on dental wax in an uncovered petri dish for 12 min, rinsed with distilled water and dried. Then stained with lead citrate on dental wax in a covered petri dish for 5 min, and rinsed with distilled water again, dried and stored. When sample and slide preparation was complete, we verified that the location of sectioning was from the EDL. Although muscle verification was performed, since the actual sectioning was done out of house, whether the slides are from the exact same location of the EDL could not be verified. To correct for this multiple slides from multiple animals were obtained. Images were captured at 1600X, 8000X, 12500X or 25000X using a Ziess 10 CA electron microscope at a voltage of 60 KV (Ziess Electron Microscopy, Thornwood, NY) on a AMT 4.10 & PCDIG side mount camera using the AMT V601 Image Capture Engine software (Advanced Microscope Technologies, Woburn, MA).

Statistical analyses

Data were presented as means ± standard error of the mean (S.E.M.). Tests of fixed effects for postnatal growth performance were analyzed using the Mixed Procedure in SAS (SAS Institute, Cary, NC). All other data were analyzed using ANOVA followed by Tukey HSD multiple comparison of means in JMP (SAS Institute, Cary, NC). Statistical significance was determined as $P < 0.05$; tendency for statistical significance was determined as $0.05 \leq P < 0.10$.

Results

Genotype ratios, gross morphology, and perinatal death

Homozygous Stac3 mutant (Stac3-/-) mice died immediately prior to, or following birth, and remained in a fetal position with limp limbs, but with no signs of edema (Figure 9). Stac3 -/- mice showed no movement at birth and failed to respond to prodding or any other form of stimulation at P0 or E17.5. Of mice born alive 74.5% were heterozygous for the Stac3 allele (Stac3+/-), 25.5% wild type (Stac3+/+), and 0% were Stac3-/-. Approximately 70.0% of mice dead at birth were Stac3-/- with 30% either Stac3+/- or Stac3+/+. However, mice from heterozygous parents at embryonic day 14.5 (E14.5) to E18.5, 46.8% were Stac3+/-, 26.9% Stac3+/+, and 26.3% Stac3-/- (Table 1). Furthermore, no mummified Stac3-/- fetuses were recovered from dissections or births.

Body weight

At E18.5, Stac3-/- mice weighed 11.2 or 13.6% less ($P < 0.0001$) than Stac3+/- or Stac3+/+, respectively. Whereas at E17.5, the body weight of Stac3 null mice were only 8.1% less ($P = 0.019$), than Stac3+/- and no difference was evident when compared to wild type (Figure 10). At E15.5 there was no difference ($P = 0.840$) in weight between Stac3-/- (0.378 ± 0.032g), Stac3+/- (0.387 ± 0.008g), and Stac3+/+ (0.373 ± 0.014g).

To determine if loss of one Stac3 allele affected growth after birth, we monitored postnatal weight gain in wild type and heterozygous Stac3 mice. Overall, there was no difference ($P = 0.7388$) between Stac3+/- and Stac3+/+ mice from weaning (three weeks of age) to sexual maturity (six weeks of age) (Table 2). Generally, there was no difference between genotypes within gender over time except between male Stac3+/- and Stac3+/+ mice at week three ($P = 0.013$). This difference, however, disappeared over time and was not observed in females.

Macromorphology

Given the neonatal mortality of Stac3-/- mice combined with the preferential expression of Stac3 in skeletal muscle, we next investigated the histological morphology of the skeletal muscle in the *extensor digitorum longus* (EDL) muscle of the lower leg (or *crus*) from both transverse (cross) and sagittal (longitudinal) sections (Figures 11and 12). Gross anatomical observations reveled severe deformities in P0 Stac3-/- skeletal muscle compared to Stac3+/+ or Stac3+/- littermates. We also examined other skeletal muscles such as the diaphragm and tongue to verify the defect was consistent across all skeletal muscles. The diaphragm appeared slightly smaller with disordered myofiber structure compared to Stac3+/+ and Stac3+/- littermates. The muscle structure of the tongue also appeared to be highly disordered having muscle fibers with abundant, centrally located nuclei (Figure 13). In control mouse muscles, often as many as three or more myofibers surrounded and contacted a single, most probably a primary, myofiber, to form a fiber bundle. In Stac3-/- mice, secondary myotubes or myofibers were more dispersed leading to more interstitial space in Stac3-/- muscles than in control muscles.

There were no obvious aberrations in any other organ systems. Special attention was given to other types of muscle such as smooth and cardiac. There was no observed defect in smooth (data not shown) or cardiac muscle (data shown). In whole body cross sections, Stac3-/- pups displayed normal cardiac cell structure and valves. Vital organs such as liver, thymus, and skeleton were largely unaffected by deletion of Stac3 (Figure 14).

Ratios of myotubes to myofibers

Cross sectional analyses of P0 Stac3-/- muscle revealed a disproportional number of centralized nuclei compared to P0 control muscle (Figure 15). Nearly all myonuclei were centrally located in P0 Stac3-/- skeletal muscle, whereas centrally located myonuclei were rare in

P0 control muscle. In muscle of P0 Stac3-/- mice, approximately 70.0% of myosin heavy chain (MyHC) positively positive cells were myotubes, which had centrally located myonuclei present or an open core. This was a 59.0% increase ($P < 0.0001$) over that in muscle of P0 Stac3+/- or Stac3+/+ mice in which only 11.0% of MyHC positive cells were myotubes. At E17.5, the percentage of MyHC positive cells differed ($P = 0.0002$) and was 95.7% in Stac3-/- pups compared to 67.3% or 76.0% in Stac3+/- or Stac3+/+ fetuses, respectively (Figure 16). The percentage of myotubes decreased by 60.7% in Stac3+/- and Stac3+/+ fetuses from E17.5 to P0; however, it decreased by only 25.7% in Stac3-/- fetuses during the same period. These results suggest myonuclei in the Stac3-/- pups failed to migrate from the center of the myotube to the periphery of the fiber.

Fiber cross sectional area and total fiber number

Compared to control pups, P0 Stac3-/- pups had a greater percentage of myofibers with extremely large cross sectional area (CSA). At P0, there was a 20% increase ($P = 0.0004$) in the average CSA in Stac3-/- mice compared to Stac3+/+ or Stac3+/- mice (Figure 17). As a result, distribution in CSA in Stac-/- mice was skewed to the right. Analysis of the EDL in Stac3-/- mice discovered 26% of fibers were greater than 90 μm^2 in diameter compared to only 4% in muscle of Stac3+/+ and Stac3+/- mice (Figure 18). At E17.5, there was also a difference in CSA in fibers of the EDL. Fibers in muscle of Stac3-/- mice measured approximately 18% greater ($P = 0.03$) than those in Stac3+/- and Stac3+/+ mice which is similar to the difference at P0 (Figure 17). E17.5 Stac3-/- fibers displayed a slight bimodal distribution in CSA, with peaks between 35 and 55 μm^2 and between 65 and 85 μm^2 in diameter with 20% of Stac3-/- fibers greater than 80 μm^2 in diameter compared to only 5% of controls (Figure 19). At P0 Stac3-/- mice had fewer fibers in the EDL than Stac3+/- or Stac3+/+ mice. At E17.5 no difference in total fiber number

was detected between any genotype. However, there was a tendency for Stac3+/+ to have more ($0.05 \leq P < 0.10$) fibers than Stac3-/- mice (Figure 20). Interestingly, the difference in total fiber number was not reflected in the overall size of the muscle where no difference ($P = 0.2$) in the mean CSA of the muscle at the widest girth in P0 or E17.5 mice was detected.

Myonuclei density

Based on analysis of longitudinal sections, Stac3-/- mice had 4.49 ± 0.45 (n = 6) nuclei per 50 μm of myofiber length. This was different ($P = 0.009$) from Stac3+/+ and Stac3+/- mice which had 2.77 ± 0.25 (n = 5) and 3.02 ± 0.22 (n = 4) nuclei per 50 μm of myofiber, respectively. This is an approximately 35% increase in nuclear density over littermate controls. The myonuclei in control mice were primarily located on the periphery of the fiber whereas the nuclei of Stac3-/- were chiefly located in the center of the myotube. The close proximity of the nuclei in the center of Stac3-/- mouse myotubes was readily evident from longitudinal sections and the phenotype was exacerbated in muscle fibers near the tendon of the *tibialis anterior*, with nuclei being aligned in a flattened elliptical formation in the myotube (Figure 12).

Subcellular structure

Using Transmission Electron Microscopy (TEM), we investigated sarcomere structure, size, and distribution in P0 and E17.5 mice. Additionally, we examined the myonuclei and their size variability (anisokaryosis), chromatin composition and location (Figure 21). Although no difference in sarcomere lengths were detected ($P = 0.23$), photomicrographs revealed disordered sarcomeres to such an extent that the width was immeasurable and an accurate estimate of the M-line width in Stac3-/- mice was not possible. At P0, control mice had very distinct and robust sarcomeres with uniform myofibrils throughout the myotube. Conversely, Stac3-/- exhibited blurred I-bands indicative of streaming Z-lines and often indistinguishable H-zones within the A-

band as well as disruption of the myofilament structure within sarcomeres. Photomicrographs also confirmed the central localization of the nuclei. Control mice displayed moderate anisokaryosis with open nucleoli. On the contrary, the Stac3-/- pups had marked anisokaryosis with less open nucleoli. Stac3-/- mice displayed increased peripheral heterochromatin indicating they had less active nuclear DNA. Albeit Stac3-/- exhibited increased heterochromatin, they did not show edema or lysis typically associated with cell death. These data suggest that the nuclei in Stac3-/- muscle were still capable of transcribing DNA, only in a primarily quiescent state. Granulated glycogen was detected in both the Stac3-/- and control mice indicating energy availability was not a cause of death. There were noticeable vacuoles in control and Stac3-/- mice, but this was attributed to artifacts that accumulated during sample collection and preparation and bared no effect on results. Photomicrographs of E17.5 mice exhibit much the same features as the P0 mice. It is evident that both Stac3-/- and control muscles were in a more immature state at E17.5 compared to P0. There was less difference in anisokaryosis between Stac3-/- and control muscles at E17.5, but difference in sarcomere structure was noticeable.

Discussion

We studied the effect of Stac3 inactivation through the gene trap method in mice. No viable Stac3-/- mice were observed following birth. When dissected out of the uterus, these pups did not respond to stimulation such as prodding and remained in a fetal position with limb limbs and symptoms of kyphosis compared to Stac3+/+ and Stac3+/- littermate pups. Additionally, genotype ratios *in utero* (E14.5 – E18.5) displayed normal Mendelian segregation suggesting the Stac3 gene product is not critical for implantation or early developmental events. Other principal phenotypes associated with inactivation of Stac3 included (1) reduced late fetal weight, (2) increased percentage of myotubes with centrally located nuclei or an open core, (3) increased myofiber CSA, (4) decreased total number of immunoreactive MyHC fibers (5) absence of fiber bundling, (6) deformed sarcomeres at the subcellular level, and (7) overall disorder about the skeletal muscle. It is likely because of these deformities the skeletal muscle was unable to function properly in Stac3 deficient mice.

Stac3 mRNA is abundantly expressed in skeletal muscle. Gene expression analysis did not detect Stac3 mRNA transcripts in any other tissues (including heart, intestine, liver, and lung) with the exception of very low levels in fetal brain samples at E17.5 (Figure 8). Additionally, expression of Stac3 in C2C12 cells *in vitro* supports Stac3 expression in skeletal muscle (unpublished data). These results substantiate our finding that there was no obvious aberration in any other organ system at P0 or E17.5. There is no detectable difference in phenotype prior to E17.5 in Stac3-/- mice compared to littermate controls. However, even though Stac3-/- mice fail to respond to stimulation, there is no evidence of edema or necrosis which is typically associated with *in utero* death. The mice appear paralyzed with fibers unable to function properly. Moreover, there are no well-documented instances of fetal death between E16

and birth (Copp, 1995). These results combined with no difference noted between Stac3-/- and control littermates prior to E17.5 lead to the conclusion Stac3-/- mice die immediately before birth, or immediately after when they become independent of maternal oxygen supply and dependent on skeletal muscle contraction of the diaphragm for oxygen intake (Copp, 1995; Turgeon and Meloche, 2009).

Interpreting the phenotypic results of Stac3 inactivation remains speculative as no obvious mechanism has yet been identified. Inactivation of Stac3 appears to have no detrimental effects on initial myotube formation. Therefore Stac3 inactivation might hinder maturation of the myotubes to form functional muscle fibers or there is an upstream function of Stac3 that prevents proper muscle fiber development which is exhibited in the late fetal period. In other words, whether Stac3 is critical only in the late fetal period when the phenotype is observed, or if it is necessary prior to the exhibition of the phenotype is not yet clear.

Based on our results, a normal muscle phenotype appears across genotypes as gestational age decreases. As mice grow from E17.5 to birth the percentage of myotubes decreased by approximately 60% (70% to 11%) in controls compared to only 25% (95% to 70%) in Stac3-/- mice. The fact that nuclear location is the most extreme phenotypic effect, Stac3 might play a role in the peripheral migration of the nuclei and therefore may halt the development of the fibers. Considering there is no detectable difference at E15.5 and the phenotype appears to rapidly progress from E15.5 Stac3 might have an important role in the late fetal period and is preventing maturation of the myotubes.

Alternatively, there might be an upstream causative effect that is only primarily exhibited during the late fetal period. Increased myonuclei per myotube or fiber supports an upstream origin. Stac3-/- mice have almost 50% more myonuclei than do control littermates with an

average of 4.5 myonuclei per 50 μm of myotube compared to 2.8 and 3.0 in controls. This demonstrates how closely the myonuclei are positioned within the myotube. On average, the nuclei in mammalian cells are approximately 6 μm in diameter (reviewed by Alberts, 2008). Vassilopoulos et al. (1976) found the typical skeletal muscle nucleus to have an average diameter of 5.4 μm in 2.4 year-old human subjects. The nuclei density observed here is supported by a parallel *in vitro* study with C2C12 cells (results discussed in separate report). This indicates that Stac3 might cause more nuclei to fuse into a single myotube, an event that takes place well before the observed phenotype (approximately at E13 in mice). The decrease in total fiber number in Stac3-/- mice might be explained by the myonuclear density. For instance, if inactivation of Stac3 causes more myoblasts to fuse into myotubes this would deplete the myoblast population. Fewer myoblasts available to fuse into myotubes would reduce the number of primary fibers. The increased density might also have a detrimental effect on the structure of the cytoskeleton preventing the proper function of cytosolic trafficking filaments and impeding proper migration of the nuclei to the periphery of the fiber. The reduced fiber number could be the result of fewer secondary fibers as well. However data determining fiber origin in Stac3-/- mice (whether primary or secondary) has not been completed at this time.

Also, the increased CSA observed does not necessarily point to a late gestational event. In Stac3-/- mice the mean CSA is 20% greater than in control littermate mice (Figure 17). In order for such an increase in CSA to be observed, an event prior would be more probable for the increased CSA to be evident. This increase in CSA is able to compensate for the decrease in fiber number in the muscle resulting in no overall change in the size of the muscle. There are several possible reasons for the increased CSA, which include increased myonuclei, or increased protein synthesis in the myotubes. Alternatively, the increased CSA might be a byproduct of other

pathological origins. It is obvious the organization of the fibers is severely distorted, but it also appears that the fibers are shortened based on longitudinal sections (Figure 12). This observation could be caused by the overall disorder of the fibers. With fewer fibers, yet unaffected overall muscle size, there appears to be more interstitial space combined with less fiber bundling that could allow for greater spatial liberty for the fibers. These fibers might weave in and out of the section plane. Another possibility is the fibers are not inherently short, but possibly become detached upon contraction. This could cause the fiber to appear shortened even though they are more so contracted giving a compact appearance with shorted length and increased CSA. This might indicate Stac3 has a role in the extracellular makeup of the fibers and functions in cell-cell interactions or adhesion. However, we did not detect a difference in sarcomere lengths from electron micrographs, which does not support the notion that the fibers are hyper contracted.

Previous studies show the two other members of the Stac family, Stac and Stac2, are expressed in a specific population of neurons in the dorsal root ganglion (Legha et al., 2010). It remains to be determined whether Stac3 has a function in, or relating to, nervous tissue, but innervation is a critical event during myogenesis. When primary fibers first form, both proliferation and hypertrophy occur, and innervation plays a significant role in both. Fernandes and Keshishian (1998) discovered that the pool of myoblasts is reduced if denervation is performed prior to fiber formation. When primary fibers form, they are initially polyneuronally innervated. The first synaptic contact on a myotube results in a convergence of several inputs onto a single myotube. In most instances, all but one input is eliminated over time resulting in just one input per myotube, typically in the middle region of the myotube, through a process called synapse elimination (Bate, 1990; Duxson, 1992; Sanes and Lichtman, 1999). However, some more recent research points to more than one innervation site, or end plate, in some muscle

fibers (Lateva et al., 2002). Nerve terminals on primary fibers regulate secondary myotube formation. Ross et al. (1987) discovered the sites of innervation on primary fibers stimulate mitosis in a nerve-dependent population of myoblasts. This suggests that the presence of nerve terminals on primary fibers is important for secondary fiber formation. Indeed it is at these sites of innervation that secondary myotubes begin developing and myogenin expression is noted (Duxson and Sheard, 1995).

There appears to be a role for innervation in primary fiber development as well. If innervation is blocked in mouse or rat limb, or is denervated before primary fiber formation, muscles form normally, but there are reduced numbers of primary and fetal muscle fibers (Harris et al., 1989; Hughes and Ontell, 1992; Phillips and Bennett, 1984; Wilson and Harris, 1993). Although innervation is not absolutely required for primary fiber formation, if innervation does not occur the primary fibers do not persist. Similarly, secondary fibers form if innervation does not occur, but with marked reduction in number of secondary fibers, and innervation is needed for secondary fiber formation to continue (Fredette and Landmesser, 1991). Also, secondary fiber hypertrophy is affected by innervation and is likely true with primary fibers as well. Research shows slow fibers of primary origin undergo severe atrophy in the absence of innervation; the same is true of secondary fibers (Crow and Stockdale, 1986; Sandri and Carraro, 1999). It is possible that the innervation event is inhibited in Stac3-/- mice causing atrophy of the primary fibers and reduced secondary fiber number. Symptoms of both appear in histological analysis with increased number of centrally located myotubes and some fibers having extreme CSA combined with the reduced overall number of fibers. Although we were unable to identify the neuromuscular junction on photomicrographs and have no direct evidence regarding inhibition of secondary fiber formation in this study, the time of nerve innervation and beginning

of secondary fiber formation is intriguing. Secondary fiber formation occurs just prior to the developmental point that the Stac3 phenotype is exhibited. Furthermore, immediate postnatal death is a frequent result of gene mutations affecting the neuromuscular junction (Turgeon and Meloche, 2009). These data suggest the possibility that Stac3 inactivation may be inhibiting a neuromuscular interaction necessary for proper development of skeletal muscle.

The possibility of fiber atrophy might indicate a pathological condition as well. At no time point during our study did normal fibers (from control littermates) possess such a large CSA in development as Stac3-/- mice. The extreme CSA in some myotubes and exacerbated phenotype in the *tibialis anterior* resembles some myopathic conditions. Centronuclear myopathies (CNM) are congenital myopathies with primary histological features being high incidence of centrally placed nuclei with 30 to 95 percent of fibers having centrally located nuclei (Engel and Franzini-Armstrong, 1994; Spiro et al., 1966). Another name given to this type of disease is type I fiber hypotrophy with central nuclei (Engel et al., 1968). Resembling CNM, the Stac3-/- muscles had long chains of nuclei in the center of the fibers. Other structural changes such as increased adipose tissue separating fasciculi are also displayed in CNM, which is similar to the Stac3 phenotypes (Engel and Franzini-Armstrong, 1994). There are many forms of CNM. The Stac3 inactivation induced phenotype resembles the Congenital Sex-Linked Myotubular Myopathy especially. It is caused by a deletion in the gene myotubularin which is a phosphatase capable of dephosphorylating phosphorylated serine and tyrosine residues (Cui et al., 1998). It has been implicated in signal transduction pathways which are involved in muscle development (reviewed by Laporte et al., 2000). Clinical features of this form of CNM include respiratory distress that is linked to weak diaphragm muscles. This myopathy causes a high mortality rate in children (Heckmatt et al., 1985). Pathological features show smaller than normal fibers among

scattered large fibers with centrally located nuclei or a clear central core zone (Engel and Franzini-Armstrong, 1994). The mortality rate and scattered large fibers is particularly suggestive of the Stac3 mutation. Central Core Disease (CCD) is another disease that exhibits centrally located nuclei or open cores. CCD has been genetically associated with mutations in the skeletal muscle isoform of the ryanodine receptor (Robinson et al., 2006). This myopathy displays jagged and streaming Z-lines when analyzed at the subcellular level, again a feature of Stac3-/- mice. These similarities provide evidence that Stac3 inactivation might facilitate a myopathological condition.

Photomicrographs obtained from Transmission Electron Microscopy (TEM) revealed several qualitative differences between control offspring and mutants such as streaming Z-lines indicated by blurred I-bands, and indistinguishable or absent M-lines in the sarcomere (Davies and Nowak, 2006). Anisokaryosis, fewer open nucleoli and dense peripheral nuclear heterochromatin was also noted in the mutant muscle. The nucleolus is site of ribosomal RNA synthesis. This indicates the processing of ribosomal RNA. Open nucleoli are indicative of an actively transcribing nucleus or could also signify the nucleus is preparing to divide (reviewed by Raska et al., 2004). The anisokaryosis was not the result of mortality. Dead nuclei are discernible by edema, disassociation of organelles, or lysis which was not present in the Stac3-/- pups. Overall, the nucleolar organization of Stac3-/- mice was different from controls, but reveals little about the potential cause of this gene deletion lethality.

The essential role of Stac3 in proper skeletal muscle development raises the question of potential mechanisms underlying the function of Stac3. Contrary to the master regulators of myogenesis, the MRFs, Stac3 is not a transcription factor in regards to DNA-binding capacity. However, Stac3 does maintain two domains (SH3 and C1) that are common components of

second messenger signal cascades. Mutations in proteins containing either C1 domains or SH3 domains vary widely. Alteration in the C1 domain of a protein typically has a detrimental effect on protein folding, which might hide residues responsible for binding (Kazanietz et al., 1995b). Meanwhile mutation in SH3 domain severely reduces protein-protein interactions. Two type I myosins Myo3p and Myo5p (not to be confused with type II myosin which is responsible for muscle contraction) possess SH3 domains. They are thought to drive actin-dependent membrane motility. A mutation in the SH3 domains of Myo3p or Myo5p leads to severe defects in actin cytoskeleton (Lechler et al., 2000). It was determined the mutation in the SH3 domain prevented binding with multiple proteins (Evangelista et al., 2000; Geli et al., 2000). Also, the Stac3 protein is confined to the cytosolic domain of the cell with no evidence for direct kinase activity based on Suzuki et al. (1996) and Abrams and Zhao (1995), but potential association with the cellular membrane is possible. The Stac family possesses both domains making the task of dissecting the complex networks Stac3 could interact with a formidable undertaking.

Conclusions

In conclusion our results demonstrate that Stac3 is essential for proper skeletal muscle development and vitality in mice. We have produced mice with lethal muscle deformities stemming from the absence of the Stac3 gene. This study identifies Stac3 as a necessary gene for proper skeletal muscle development and vitality in mice. More research will be needed to determine the mechanism and exact role of Stac3 in skeletal muscle development.

Table 1.

Frequency of genotypes in offspring from Stac3+/- x Stac3+/- parents. Percentages indicate no live Stac3-/- offspring are capable of reaching weaning age, but normal Mendelian segregation during fetal period is present.

Age	n	Stac3+/+ (%)	Stac3+/- (%)	Stac3-/- (%)
Fetal (E14.5 – E18.5)	156	42 (26.9)	73 (46.8)	41 (26.3)
Weaning (3wks)	131	47 (35.9)	84 (64.1)	0

Table 2.

Tests of fixed effects on growth traits of Stac3+/- and Stac3+/+ mice. Data from weaning (3 wks) to maturity (6 wks). No difference in growth was detected between Stac3+/- and Stac3+/+. n = 24 for Stac3+/- and n = 13 for Stac3+/+.

Effect	Num DF	Den DF	F Value	Pr > F
genotype	1	33	0.11	0.7388
week	3	99	477.45	<.0001
genotype*week	3	99	0.85	0.4687
gender	1	33	21.73	<.0001
genotype*gender	1	33	1.11	0.2995
gender*week	3	99	21.95	<.0001
genotype*sex*week	3	99	1.27	0.2881

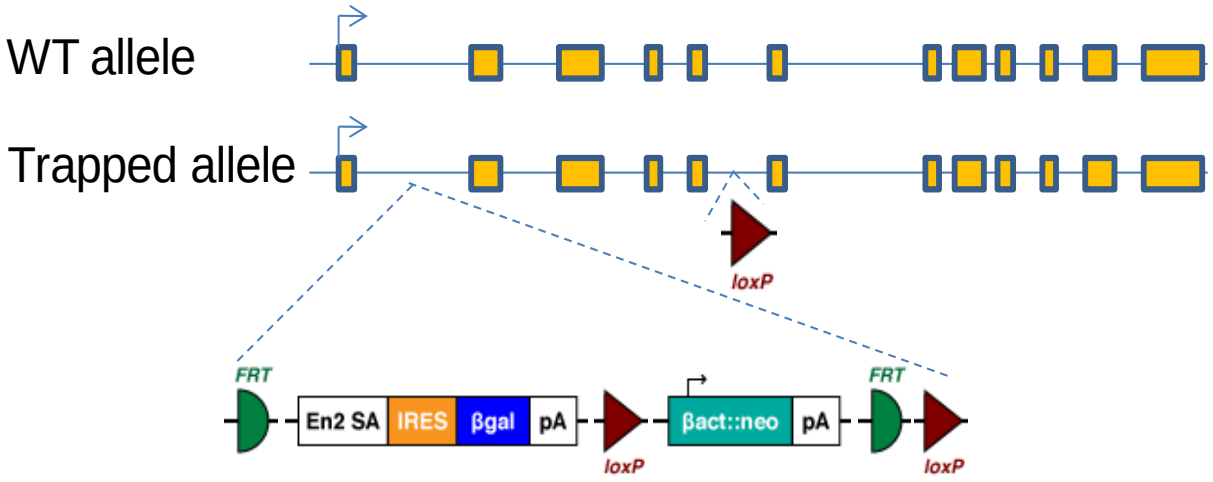

Figure 6. Schematic of the wild type (WT) and trapped Stac3 alleles. The WT Stac3 allele has 12 exons, with the third exon containing the translation start codon. The trapped Stac3 allele is inserted with a "trapping cassette" in the first intron and a third loxP site in the fifth intron.

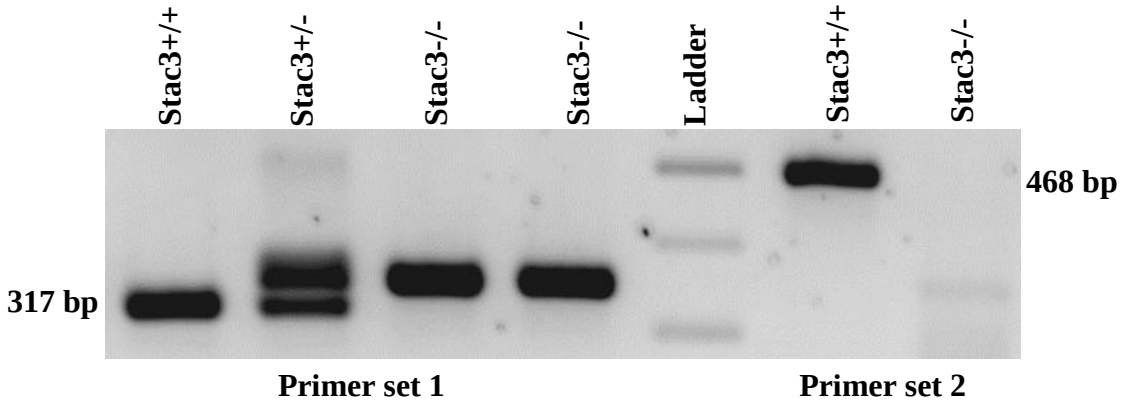

Figure 7. Electrophorese gel product of genotypes. Primer set 1 used to distinguish between Stac3+/- mice (having a product of 344 bp) and Stac3+/+ mice (having a product of 317), but was also capable of discerning Stac3-/- offspring. Primer set 2 used to distinguish between Stac3-/- (having a product > 1000 bp) and Stac3+/- or Stac3+/+ (having a product of 468 bp) mice.

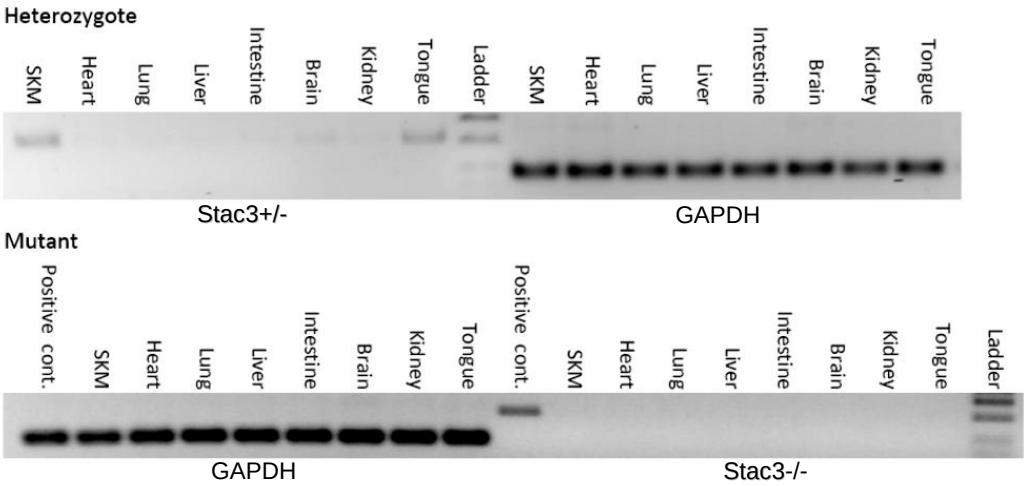

Figure 8. Stac3 expression in seven different tissues isolated from E17.5 Stac3+/- (top) and Stac3-/- (bottom) fetuses. Inactivation of Stac3 is confirmed in the bottom gel where the highly specific expression of Stac3 is evident in the top gel. Positive control was skeletal muscle (SKM) from Stac3+/+ littermate with an internal control of glyceraldehyde-3-phosphate dehydrogenase (GAPDH).

Figure 9. Representative images of Stac3-/- (left) and Stac3+/+ (right) mice at P0. Notice that the mutant had a more curved body and dropping forelimbs.

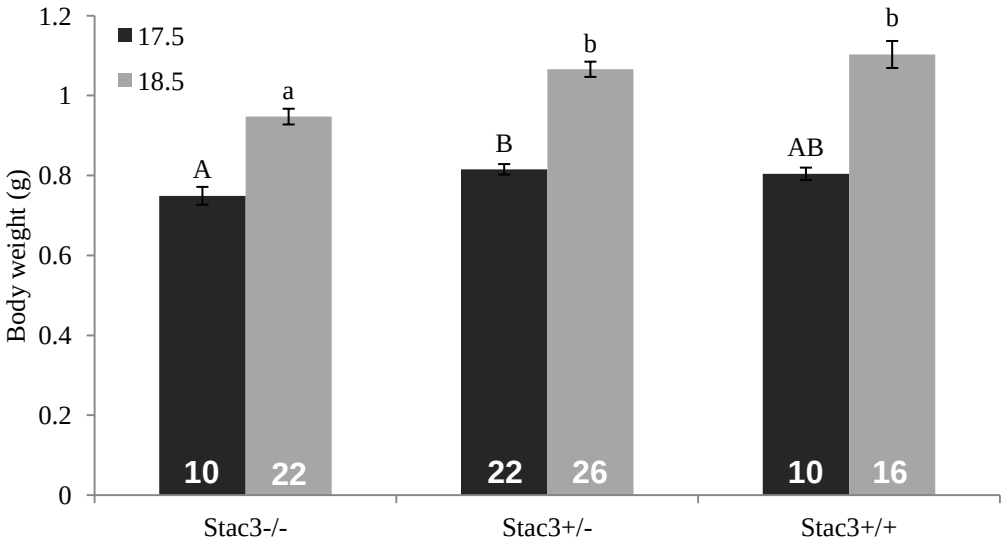

Figure 10. Body weights of Stac3-/-, Stac3+/- and Stac3+/+ fetuses dissected at E17.5 (black) and 18.5 (grey). The number of individuals per genotype (n) is indicated in the bars. Data are mean ± SEM. Means bearing different letters differ ($P < 0.05$).

+/- -/-

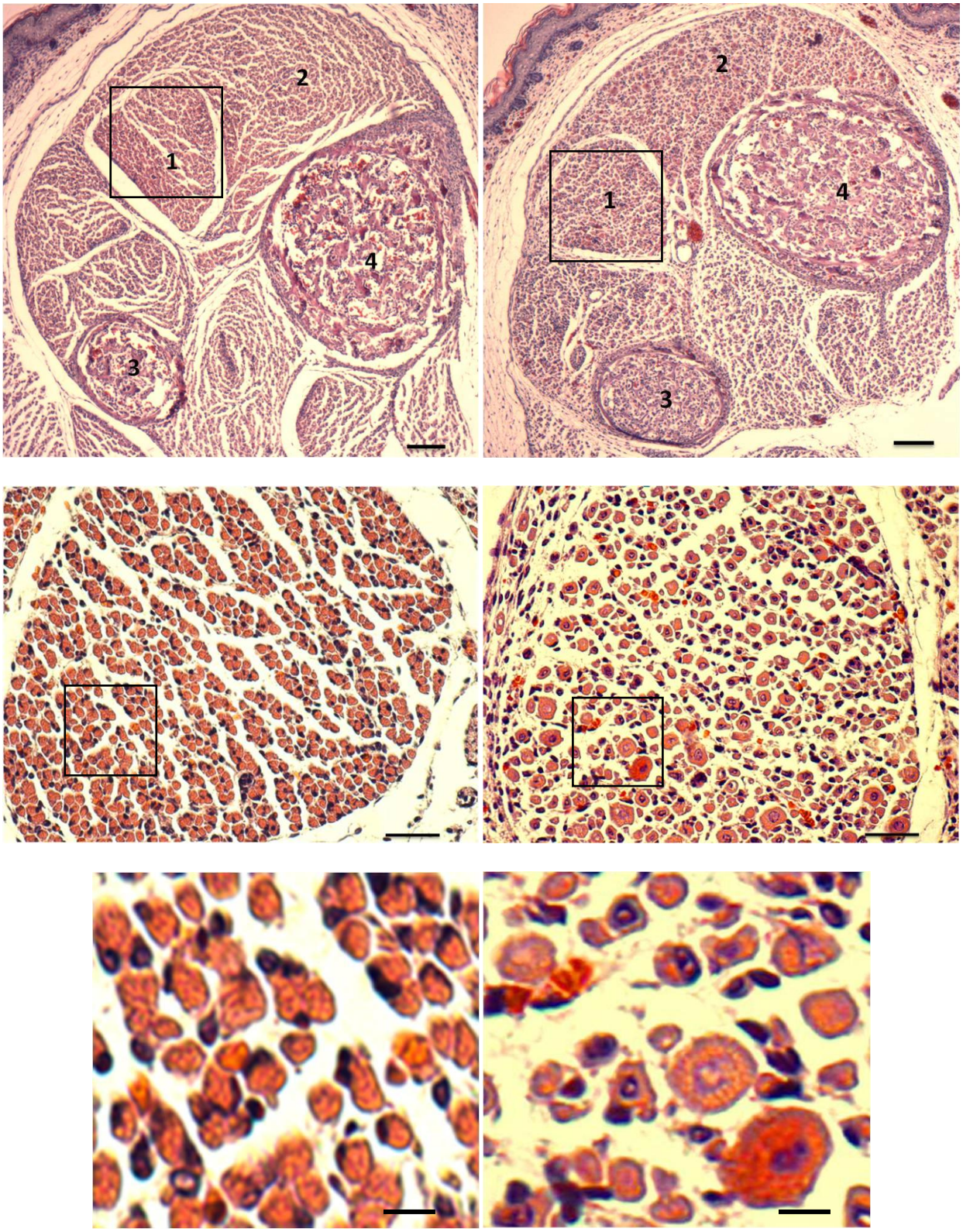
1
2
3
4
1
2
3
4

Figure 11. Representative hind limb transverse H&E stained cross-sections from P0 Stac3+/- (left column) and Stac3-/- (right column) littermates taken from approximately the same location of the lower leg (*crus*). Low magnification (top row) with reference labeled muscles (1, 2) and bones (3, 4). Label 1 = *extensor digitorum longus* (EDL) 2 = *tibialis anterior* (TA) 3 = fibula 4 = tibia. High magnification of the EDL (middle row) illustrates the disorder of the myofibers and lack of fiber bundling. Greater magnification (bottom row) denotes the extremely large and varied diameter and centrally located nuclei in the fibers of the Stac3-/- mice. Bar = 100 µm (top row) 50 µm (middle row) and 15 um (bottom row)

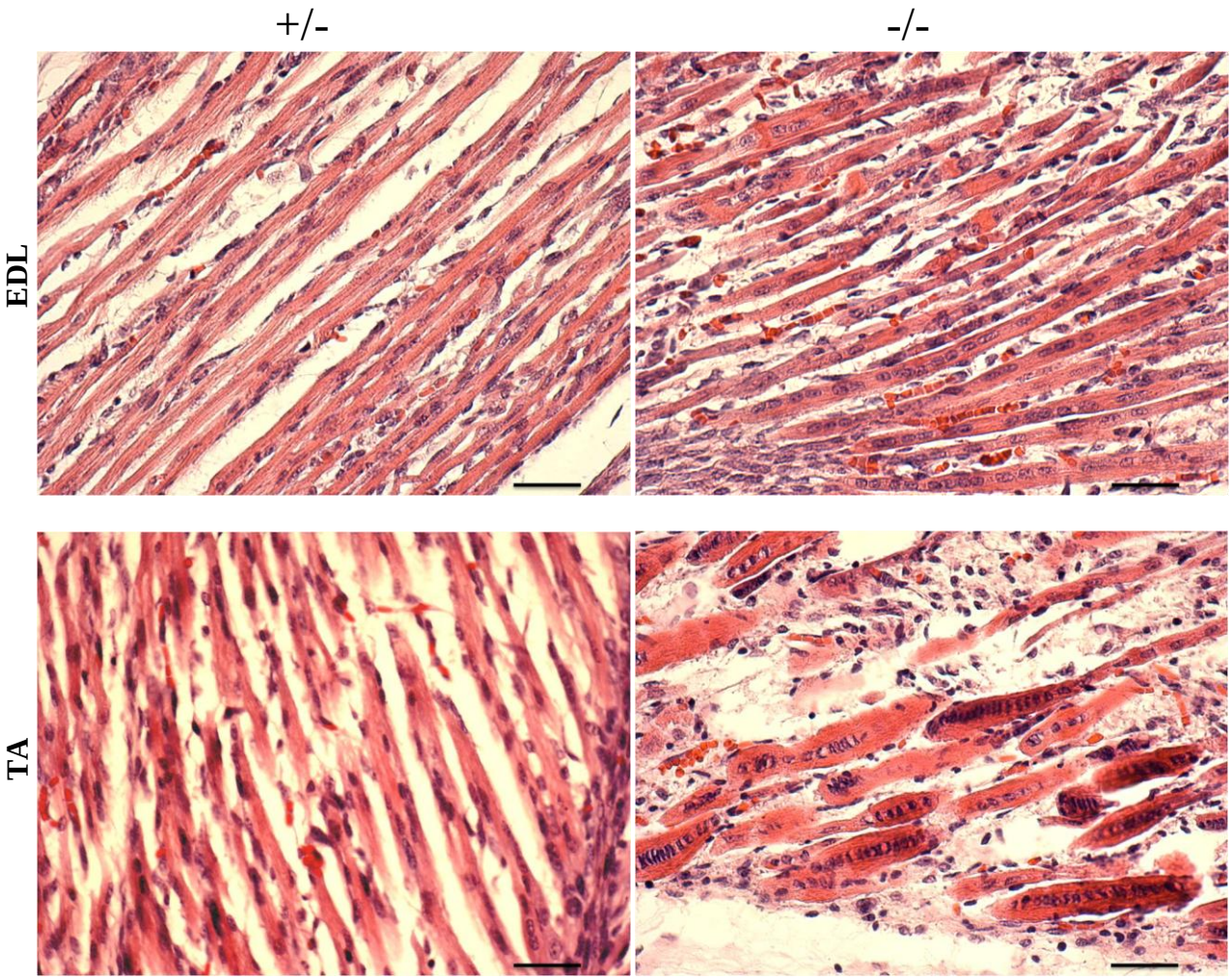

Figure 12. Sagittal sections from the *extensor digitorum longus* (EDL) (top row) and *tibialis anterior* (TA) (bottom row) in P0 Stac3+/- (left column) and P0 Stac3-/- (right column) littermates. Stac3-/- mice display centrally located nuclei and dense packing of nuclei. Stac3+/- mice show proper fiber structure where the length of a single fiber can be traced through the entire length of the image. Stac3-/- mice have disordered and shorter myotube structure. Extreme stacking of nuclei is displayed near tendon of the *tibialis anterior* of P0 Stac3-/-. The orientation of the nuclei is perpendicular to the myotube creating dense and elliptical-shaped nuclei in the center of the myotube. Bar = 50 µm.

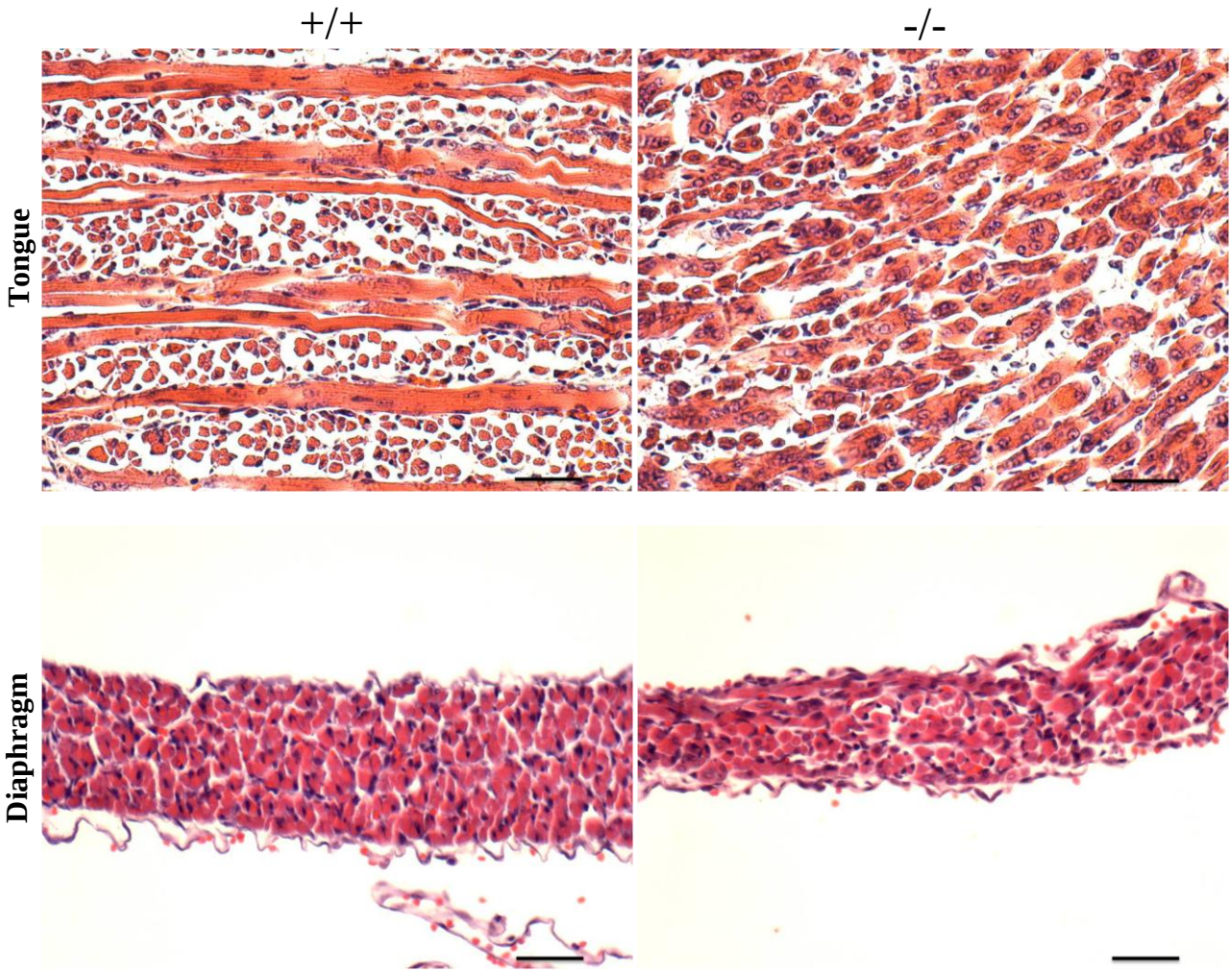

Figure 13. Representative sagittal tongue (top row) and diaphragm (bottom row) muscle cross-sections stained with H&E from P0 Stac3+/+ (left column) and P0 Stac3-/- (right column) littermates. Analysis of various skeletal muscles confirming phenotype is ubiquitous in skeletal muscle. The tongue displays severe aberrations in fiber development where as the diaphragm appears thinner. Bar = 50 µm.

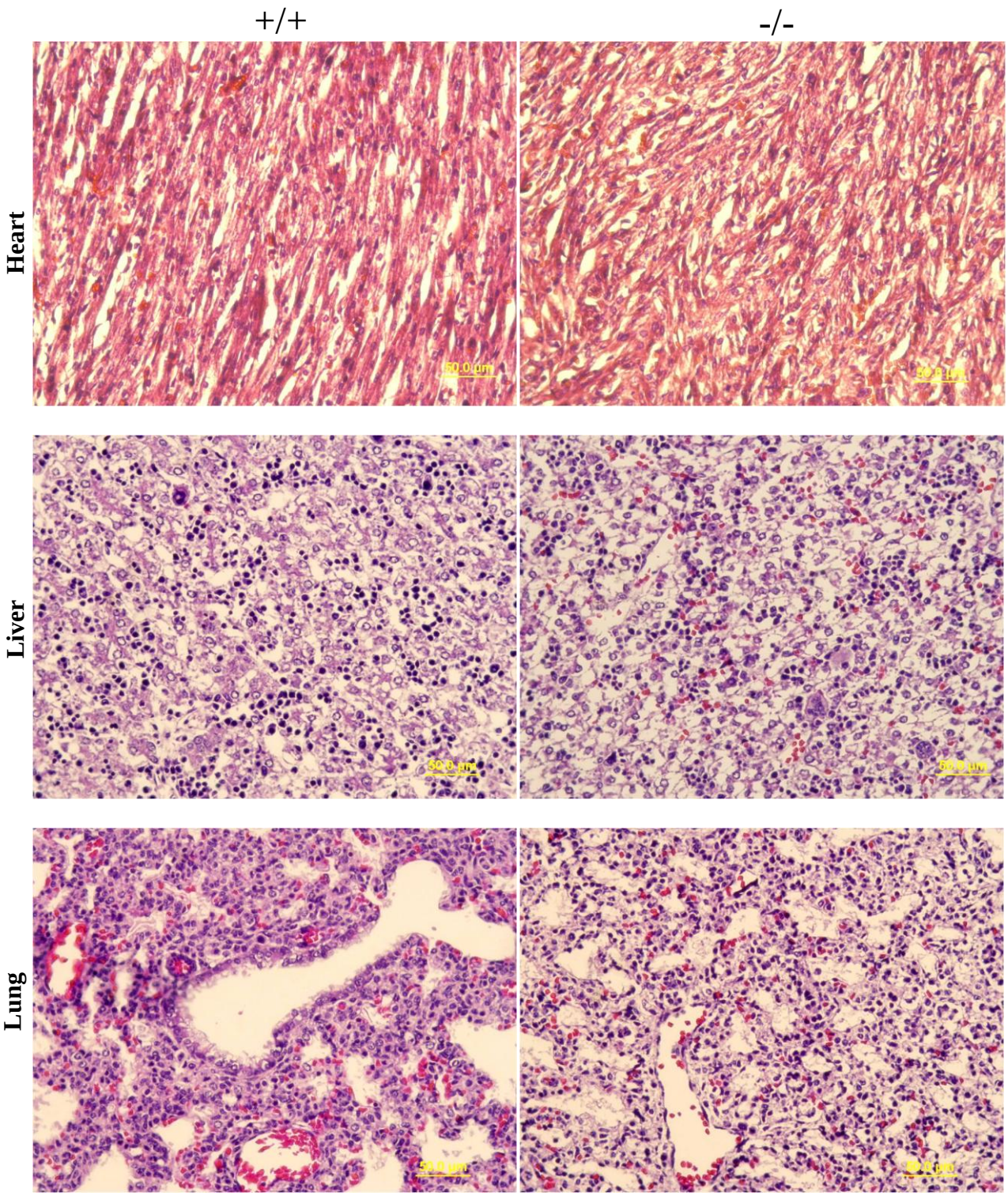

Figure 14. Cross sections of various tissues from P0 Stac3+/+ (left column) and Stac3-/- (right column) not expressing Stac3. No histological differences were detected in the heart (top row) and liver (middle row) of littermate mice. Lungs (bottom row) from P0 Stac3+/+ show expansion of alveoli indicating respiration where Stac-/- fail to display evidence of alveolar expansion. Bar = 50 µm.

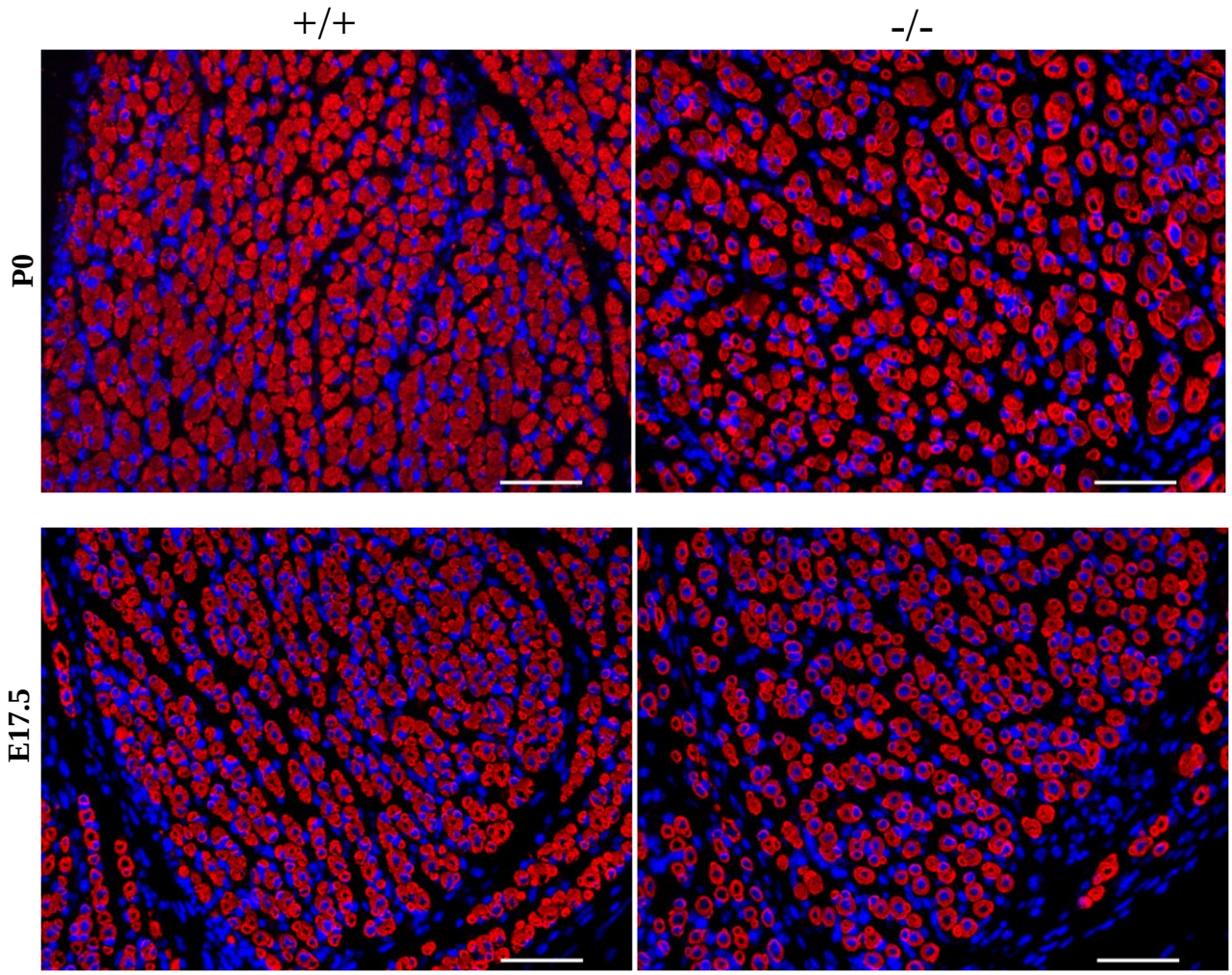

Figure 15. Imunnohistochemical (IHC) staining of myosin heavy chain protein (red) with nuclear counter stain (blue) from the *extensor digitorum longus* of Stac3+/+ (left column) and Stac3-/- (right column) littermates at P0 (top row) and E17.5 (bottom row). Bar = 50 µm.

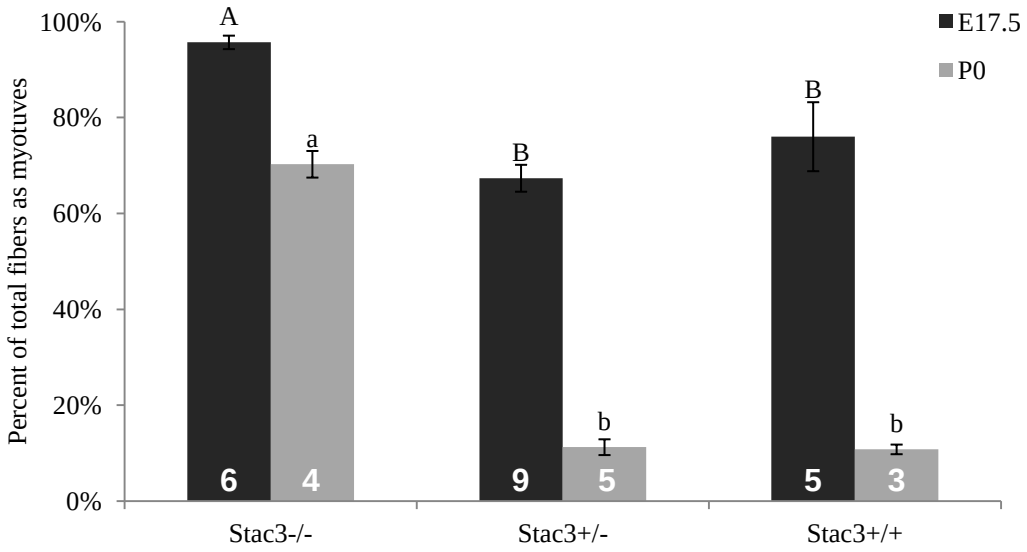

Figure 16. Percent of myotubes (fibers appearing tubular) containing immunoreactive myosin heavy chain from littermates at E17.5 (black) and P0 (grey). The number of individuals per genotype (n) is indicated in the bars. Data are mean ± SEM. Means bearing different letters differ ($P < 0.05$).

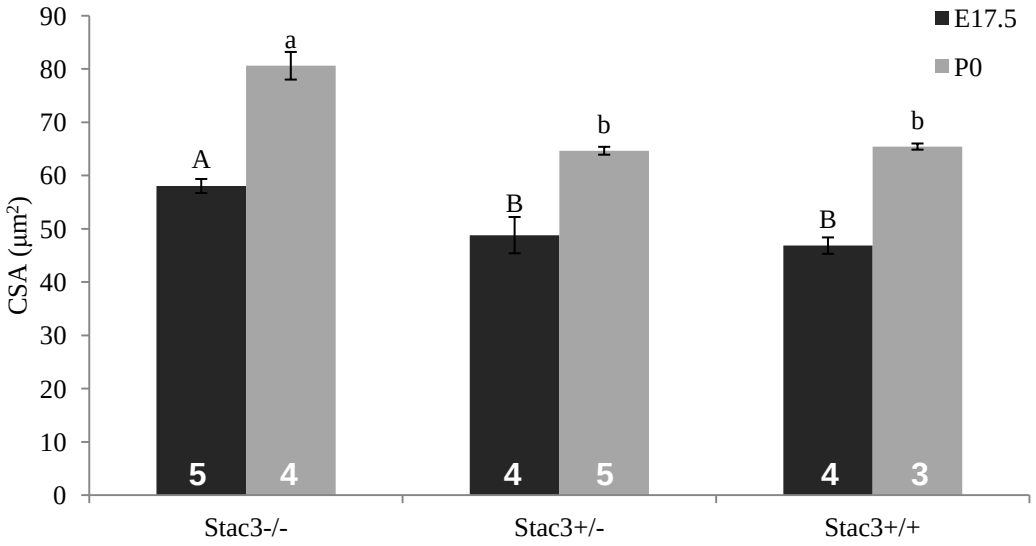

Figure 17. Cross sectional area (CSA) of muscle fibers containing immunoreactive myosin heavy chain in *extensor digitorum longus* from mice at E17.5 (black) and P0 (grey). The number of individuals per genotype (n) is indicated in the bars. Data are mean ± SEM. Means bearing different letters differ ($P < 0.05$).

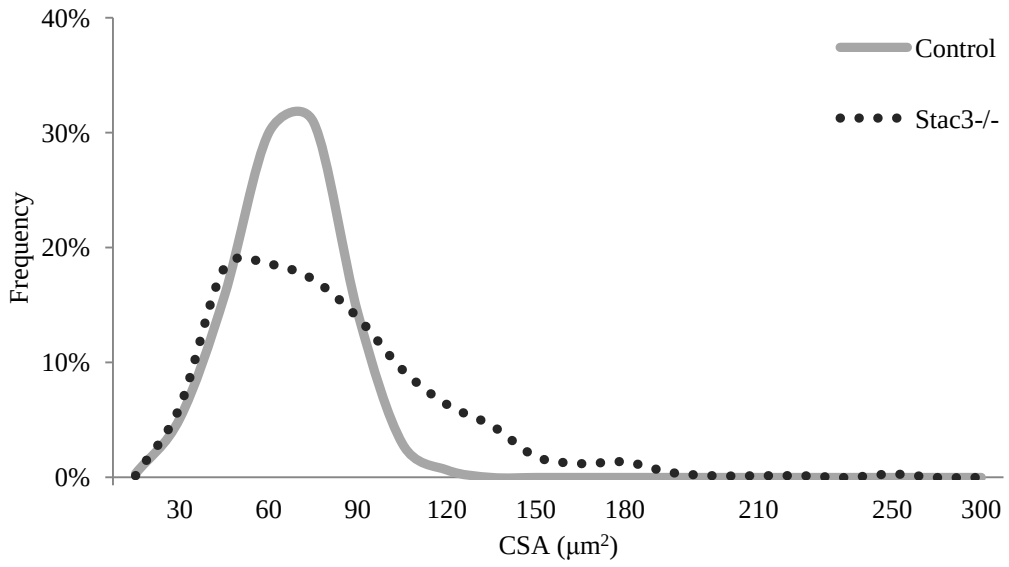

Figure 18. Frequency distribution of muscle fiber cross sectional areas (CSA) from P0 *extensor digitorum longus* of Stac3+/- and Stac3+/+ (grey line) compared to Stac3-/- (black dashed line).

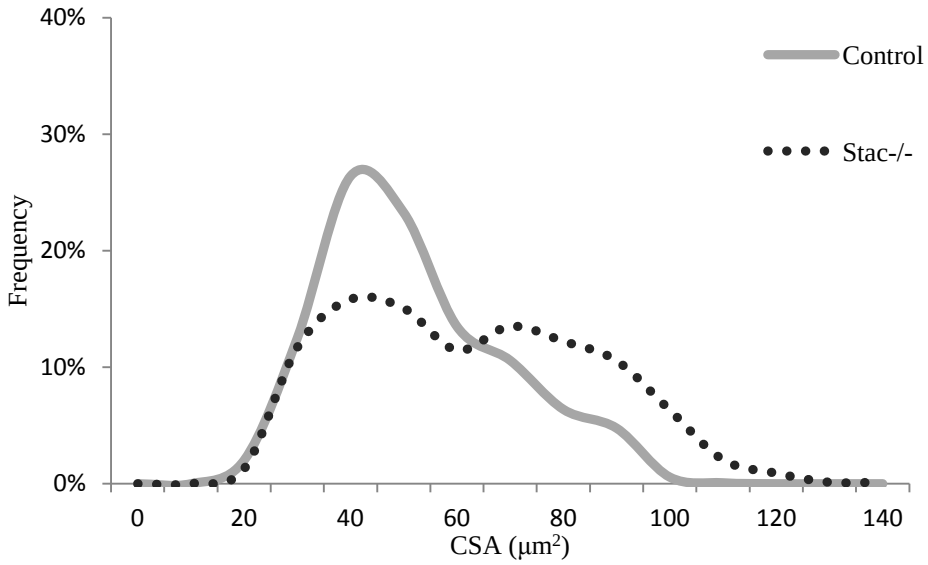

Figure 19. Frequency distribution of muscle fiber cross sectional areas (CSA) from E17.5 *extensor digitorum longus* of Stac3+/- and Stac3+/+ (grey line) compared to Stac3-/- (black dashed line). Note the bimodal peaks between 35 and 55 μm^2 and between 65 and 85 μm^2 in CSA in Stac3-/- mice.

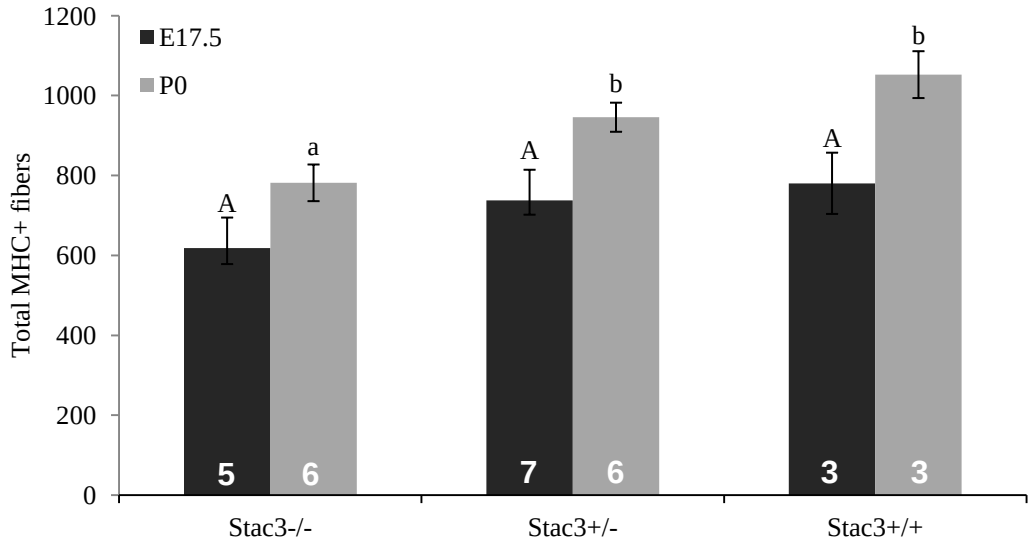

Figure 20. Total number of myosin heavy chain-positive muscle fibers possessing immunoreactive myosin in the *extensor digitorum longus* from mice at E17.5 (black) and P0 (grey). The number of individuals per genotype (n) is indicated in the bars. Data are mean ± SEM. Means bearing different letters differ ($P < 0.05$).

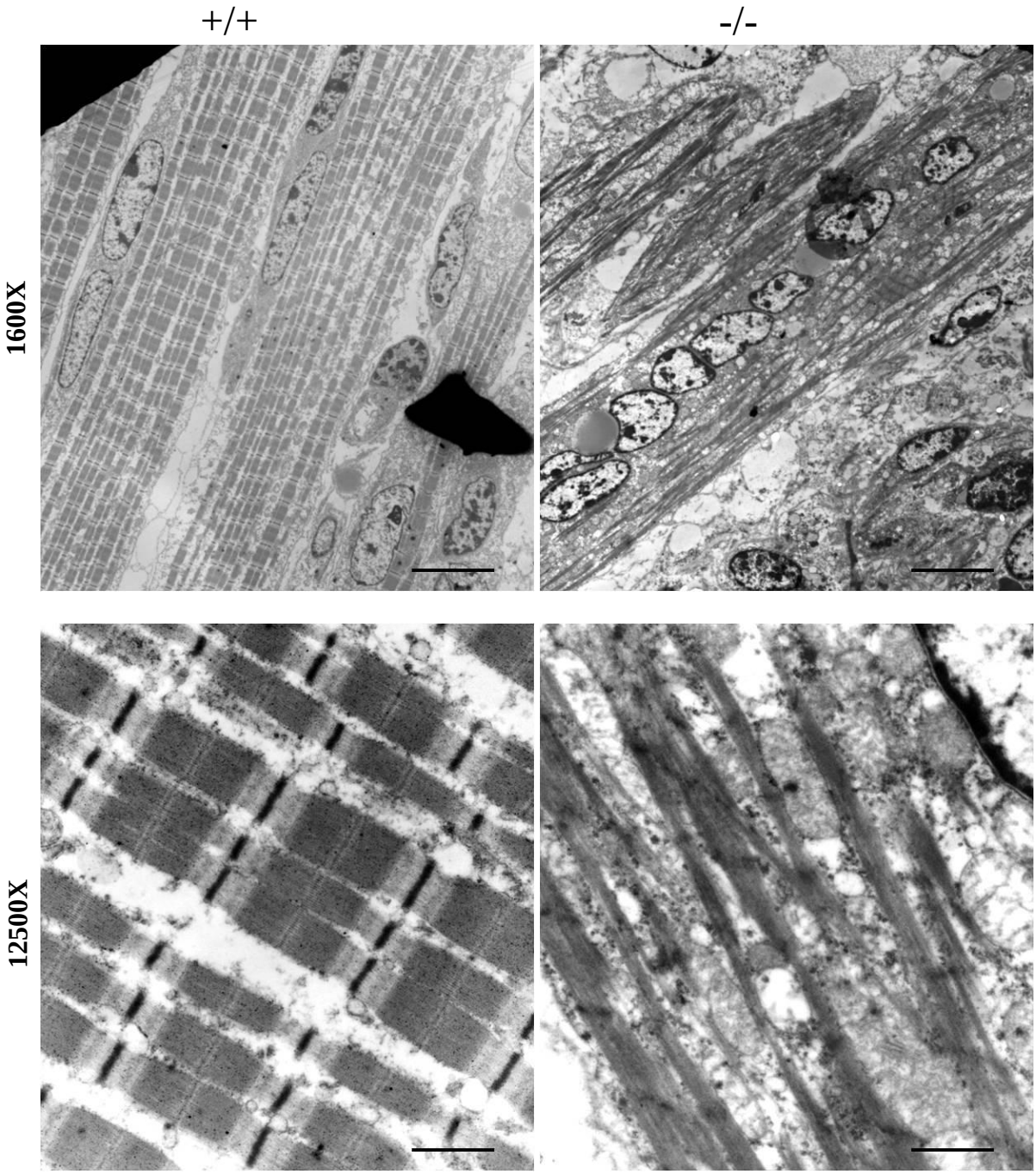

Figure 21. Electron micrographs of muscle from the *extensor digitorum longus* of Stac3+/+ (left column) and Stac3-/- (right column) from P0 littermates. Bar = 10 µm (top row) and 500 nm (bottom row).

CHAPTER III

Future objectives

The novelty of this project allows for many potential directions for future research objectives. Certainly the most unique feature the Stac3-/- mouse model is the cassette inserted which prevents transcription of Stac3. The inserted cassette possesses the ability to be conditionally knocked out by first rescuing the phenotype and then later deleting at the discretion of the investigator (see Appendix A). This would provide gene inactivation in a live animal to further investigate the phenotypic effects of Stac3. Additionally, an efficient antibody to the Stac3 protein product is necessary. Although there have been some developed in the past, these have had mixed results. While some encouraging results have come from the antibody's recognition ability in some protein assays, this has not been observed in histological experiments. The ability to not only detect the Stac3 protein product, but to be able to localize the protein in histological samples would reveal a great deal about the function of Stac3 *in vivo*.

Another fundamental question that would begin to elucidate the mechanism of Stac3 action is to study what proteins interact with it within the cell. It is apparent Stac3 does not bind to DNA directly, but has potential binding sites for membrane bound second messengers. Assays such as a yeast two-hybrid screen could reveal other proteins that bind directly to Stac3 (Joung et al., 2000). Also the inserted cassette has a β-galactosidase site included in it. This can be used for Lac-z staining (using the X-gal substrate) on mutants and heterozygotes for transcript location (Watson et al., 2008). In addition, even though Stac3 tissue expression is established, *in situ* hybridization could shed more light on where Stac3 is expressed and to what level by exposing mRNA transcripts. This would be especially valuable for mapping a timeline of Stac3 expression through early development.

Primary and secondary myogenesis have different MyHC expression patterns which dictate fiber type (type I, IIa, IIb or IIx) (Pin et al., 2002). We did not look extensively at fiber types in mutant mice compared with controls. Identifying differences in fiber types could shed light on whether Stac3 is functioning in primary myogenesis, secondary myogenesis, or at another developmental time point. Also, more careful investigation into the neuromuscular junction is warranted. If Stac3 does play a role in the neuromuscular interaction, then analysis of neurotransmitters, such as acetylcholine, or monitoring downstream effects of neurological stimulation such as calcium transients, could yield great results.

Regardless of the direction pursued, identification of Stac3 as a critical gene in development marks advancement in elucidating the underlying physiological mechanisms of early development. Including Stac3 in complex molecular networks is the ultimate goal and the outlined potential future objectives would begin establishing this connection.

Literature cited

Aberle, E. D. 2001. Principles of meat science. Kendall/Hunt, Dubuque, Iowa.

Abrams, C. S., and W. Zhao. 1995. SH3 domains specifically regulate kinase activity of expressed src family proteins. J. Biol. Chem. 270: 333-339.

Alberts, B. 2008. Molecular biology of the cell. Garland Science, New York, New York.

Aulehla, A., and B. G. Herrmann. 2004. Segmentation in vertebrates: Clock and gradient finally joined. Genes Dev. 18: 2060-2067.

Bate, M. 1990. The embryonic development of larval muscles in drosophila. Development 110: 791-804.

Boettiger, D., M. Enomoto-Iwamoto, H. Y. Yoon, U. Hofer, A. S. Menko, and R. Chiquet-Ehrismann. 1995. Regulation of integrin alpha 5 beta 1 affinity during myogenic differentiation. Dev. Biol. 169: 261-272.

Bonaldo, P., K. Chowdhury, A. Stoykova, M. Torres, and P. Gruss. 1998. Efficient gene trap screening for novel developmental genes using IRES beta geo vector and in vitro preselection. Exp. Cell Res. 244: 125-136.

Borneman, A., R. Kuschel, and A. Fujisawa-Sehara. 2000. Analysis for transcript expression of meltrin alpha in normal, regenerating, and denervated rat muscle. J. Muscle Res. Cell. Motil. 21: 475-480.

Bouvier, J., and J. G. Cheng. 2009. Recombineering-based procedure for creating Cre/loxP conditional knockouts in the mouse. Curr. Protoc. Mol. Biol. Chapter 23: Unit 23 13.

Brand-Saberi, B. 2002. Vertebrate myogenesis. Springer, Berlin; Germany.

Brand-Saberi, B., and B. Christ. 2000. Evolution and development of distinct cell lineages derived from somites. Curr. Top. Dev. Biol. 48: 1-42.

Braun, T., G. Buschhausen-Denker, E. Bober, E. Tannich, and H. H. Arnold. 1989. A novel human muscle factor related to but distinct from MyoD1 induces myogenic conversion in 10T1/2 fibroblasts. EMBO J. 8: 701-709.

Braun, T., M. A. Rudnicki, H. H. Arnold, and R. Jaenisch. 1992. Targeted inactivation of the muscle regulatory gene Myf-5 results in abnormal rib development and perinatal death. Cell 71: 369-382.

Brtva, T. R., J. K. Drugan, S. Ghosh, R. S. Terrell, S. Campbell-Burk, R. M. Bell, and C. J. Der. 1995. Two distinct Raf domains mediate interaction with Ras. J. Biol. Chem. 270: 9809-9812.

Buckingham, M., L. Bajard, T. Chang, P. Daubas, J. Hadchouel, S. Meilhac, D. Montarras, D. Rocancourt, and F. Relaix. 2003. The formation of skeletal muscle: From somite to limb. J. Anat. 202: 59-68.

Buckingham, M., L. Bajard, P. Daubas, M. Esner, M. Lagha, F. Relaix, and D. Rocancourt. 2006. Myogenic progenitor cells in the mouse embryo are marked by the expression of Pax3/7 genes that regulate their survival and myogenic potential. Anat. Embryol. (Berl) 211 Suppl 1: 51-56.

Burke, A. C., and J. L. Nowicki. 2003. A new view of patterning domains in the vertebrate mesoderm. Dev. Cell 4: 159-165.

Carapuco, M., A. Novoa, N. Bobola, and M. Mallo. 2005. Hox genes specify vertebral types in the presomitic mesoderm. Genes Dev. 19: 2116-2121.

Casadaban, M. J., and S. N. Cohen. 1979. Lactose genes fused to exogenous promoters in one step using a Mu-lac bacteriophage: In vivo probe for transcriptional control sequences. Proc. Natl. Acad. Sci. USA 76: 4530-4533.

Christ, B., and C. P. Ordahl. 1995. Early stages of chick somite development. Anat. Embryol. (Berl) 191: 381-396.

Collins, F. S., R. H. Finnell, J. Rossant, and W. Wurst. 2007. A new partner for the international knockout mouse consortium. Cell 129: 235-235.

Colon-Gonzalez, F., and M. G. Kazanietz. 2006. C1 domains exposed: From diacylglycerol binding to protein-protein interactions. Biochim. Biophys. Acta 1761: 827-837.

Condon, K., L. Silberstein, H. M. Blau, and W. J. Thompson. 1990. Differentiation of fiber types in aneural musculature of the prenatal rat hindlimb. Dev. Biol. 138: 275-295.

Coolican, S. A., D. S. Samuel, D. Z. Ewton, F. J. McWade, and J. R. Florini. 1997. The mitogenic and myogenic actions of insulin-like growth factors utilize distinct signaling pathways. J. Biol. Chem. 272: 6653-6662.

Copp, A. J. 1995. Death before birth: Clues from gene knockouts and mutations. Trends Genet. 11: 87-93.

Crow, M. T., and F. E. Stockdale. 1986. Myosin expression and specialization among the earliest muscle fibers of the developing avian limb. Dev. Biol. 113: 238-254.

Csete, M., J. Walikonis, N. Slawny, Y. Wei, S. Korsnes, J. C. Doyle, and B. Wold. 2001. Oxygen-mediated regulation of skeletal muscle satellite cell proliferation and adipogenesis in culture. J. Cell. Physiol. 189: 189-196.

Cui, X., I. De Vivo, R. Slany, A. Miyamoto, R. Firestein, and M. L. Cleary. 1998. Association of set domain and myotubularin-related proteins modulates growth control. Nat. Genet. 18: 331-337.

Davies, K. E., and K. J. Nowak. 2006. Molecular mechanisms of muscular dystrophies: Old and new players. Nat. Rev. Mol. Cell Biol. 7: 762-773.

Davis, R. L., H. Weintraub, and A. B. Lassar. 1987. Expression of a single transfected cDNA converts fibroblasts to myoblasts. Cell 51: 987-1000.

Dequeant, M. L., and O. Pourquie. 2008. Segmental patterning of the vertebrate embryonic axis. Nat. Rev. Genet. 9: 370-382.

Dubrulle, J., M. J. McGrew, and O. Pourquie. 2001. FGF signaling controls somite boundary position and regulates segmentation clock control of spatiotemporal Hox gene activation. Cell 106: 219-232.

Dubrulle, J., and O. Pourquie. 2004a. Coupling segmentation to axis formation. Development 131: 5783-5793.

Dubrulle, J., and O. Pourquie. 2004b. fgf8 mRNA decay establishes a gradient that couples axial elongation to patterning in the vertebrate embryo. Nature 427: 419-422.

Durick, K., J. Mendlein, and K. G. Xanthopoulos. 1999. Hunting with traps: Genome-wide strategies for gene discovery and functional analysis. Genome Res. 9: 1019-1025.

Duxson, M. J. 1992. The relationship of nerve to myoblasts and newly-formed secondary myotubes in the fourth lumbrical muscle of the rat foetus. J. Neurocytol. 21: 574-588.

Duxson, M. J., and P. W. Sheard. 1995. Formation of new myotubes occurs exclusively at the multiple innervation zones of an embryonic large muscle. Dev. Dyn. 204: 391-405.

Ellenberger, T., D. Fass, M. Arnaud, and S. C. Harrison. 1994. Crystal structure of transcription factor E47: E-box recognition by a basic region helix-loop-helix dimer. Genes Dev. 8: 970-980.

Endo, T. 2007. Stem cells and plasticity of skeletal muscle cell differentiation: Potential application to cell therapy for degenerative muscular diseases. Regen. Med. 2: 243-256.

Engel, A., and C. Franzini-Armstrong. 1994. Myology: Basic and clinical. McGraw-Hill, New York, New York.

Engel, W. K., G. N. Gold, and G. Karpati. 1968. Type I fiber hypotrophy and central nuclei. A rare congenital muscle abnormality with a possible experimental model. Arch. Neurol. 18: 435-444.

Epstein, J., J. Cai, T. Glaser, L. Jepeal, and R. Maas. 1994. Identification of a Pax paired domain recognition sequence and evidence for DNA-dependent conformational changes. J. Biol. Chem. 269: 8355-8361.

Evangelista, M., B. M. Klebl, A. H. Tong, B. A. Webb, T. Leeuw, E. Leberer, M. Whiteway, D. Y. Thomas, and C. Boone. 2000. A role for myosin-I in actin assembly through interactions with Vrp1p, Bee1p, and the Arp2/3 complex. J. Cell Biol. 148: 353-362.

Fernandes, J. J., and H. Keshishian. 1998. Nerve-muscle interactions during flight muscle development in drosophila. Development 125: 1769-1779.

Fredette, B. J., and L. T. Landmesser. 1991. A reevaluation of the role of innervation in primary and secondary myogenesis in developing chick muscle. Dev. Biol. 143: 19-35.

Ge, X. 2012. Roles of growth hormone, insulin-like growth factor I, and SH3 and cysteine rich domain 3 in skeletal muscle growth. PhD dissertation Virginia Tech University, Department of Animal and Poultry Scienecs.

Geli, M. I., R. Lombardi, B. Schmelzl, and H. Riezman. 2000. An intact SH3 domain is required for myosin I-induced actin polymerization. EMBO J. 19: 4281-4291.

George-Weinstein, M., R. F. Foster, J. V. Gerhart, and S. J. Kaufman. 1993. In vitro and in vivo expression of alpha 7 integrin and desmin define the primary and secondary myogenic lineages. Dev. Biol. 156: 209-229.

Gilbert, S. F. 2010. Developmental biology. Sinauer Associates, Sunderland, Massachusetts.

Goodson, H. V., B. L. Anderson, H. M. Warrick, L. A. Pon, and J. A. Spudich. 1996. Synthetic lethality screen identifies a novel yeast myosin I gene (MYO5): myosin I proteins are required for polarization of the actin cytoskeleton. J. Cell Biol. 133: 1277-1291.

Gros, J., M. Manceau, V. Thome, and C. Marcelle. 2005. A common somitic origin for embryonic muscle progenitors and satellite cells. Nature 435: 954-958.

Harris, A. J., R. B. Fitzsimons, and J. C. McEwan. 1989. Neural control of the sequence of expression of myosin heavy chain isoforms in foetal mammalian muscles. Development 107: 751-769.

Hasty, P., A. Bradley, J. H. Morris, D. G. Edmondson, J. M. Venuti, E. N. Olson, and W. H. Klein. 1993. Muscle deficiency and neonatal death in mice with a targeted mutation in the myogenin gene. Nature 364: 501-506.

Hatta, K., S. Takagi, H. Fujisawa, and M. Takeichi. 1987. Spatial and temporal expression pattern of N-cadherin cell adhesion molecules correlated with morphogenetic processes of chicken embryos. Dev. Biol. 120: 215-227.

Heckmatt, J. Z., C. A. Sewry, D. Hodes, and V. Dubowitz. 1985. Congenital centronuclear (myotubular) myopathy. Brain 108: 941-964.

Horsley, V., K. M. Jansen, S. T. Mills, and G. K. Pavlath. 2003. IL-4 acts as a myoblast recruitment factor during mammalian muscle growth. Cell 113: 483-494.

Hughes, D. S., and M. Ontell. 1992. Morphometric analysis of the developing, murine aneural soleus muscle. Dev. Dyn. 193: 175-184.

Hughes, S. M., and H. M. Blau. 1992. Muscle fiber pattern is independent of cell lineage in postnatal rodent development. Cell 68: 659-671.

Ikeya, M., and S. Takada. 1998. Wnt signaling from the dorsal neural tube is required for the formation of the medial dermomyotome. Development 125: 4969-4976.

Jackson, K. A., T. Mi, and M. A. Goodell. 1999. Hematopoietic potential of stem cells isolated from murine skeletal muscle. Proc. Natl. Acad. Sci. USA 96: 14482-14486.

Joung, J. K., E. I. Ramm, and C. O. Pabo. 2000. A bacterial two-hybrid selection system for studying protein-DNA and protein-protein interactions. Proc. Natl. Acad. Sci. USA 97: 7382-7387.

Kaliman, P., F. Vinals, X. Testar, M. Palacin, and A. Zorzano. 1996. Phosphatidylinositol 3-kinase inhibitors block differentiation of skeletal muscle cells. J. Biol. Chem. 271: 19146-19151.

Kassar-Duchossoy, L., E. Giacone, B. Gayraud-Morel, A. Jory, D. Gomes, and S. Tajbakhsh. 2005. Pax3/Pax7 mark a novel population of primitive myogenic cells during development. Genes Dev. 19: 1426-1431.

Kawai, J., H. Suzuki, A. Hara, K. Hirose, and S. Watanabe. 1998. Human and mouse chromosomal mapping of Stac, a neuron-specific protein with an SH3 domain. Genomics 47: 140-142.

Kazanietz, M. G., J. J. Barchi, Jr., J. G. Omichinski, and P. M. Blumberg. 1995a. Low affinity binding of phorbol esters to protein kinase C and its recombinant cysteine-rich region in the absence of phospholipids. J. Biol. Chem. 270: 14679-14684.

Kazanietz, M. G., X. R. Bustelo, M. Barbacid, W. Kolch, H. Mischak, G. Wong, G. R. Pettit, J. D. Bruns, and P. M. Blumberg. 1994. Zinc finger domains and phorbol ester pharmacophore. Analysis of binding to mutated form of protein kinase C zeta and the vav and c-raf proto-oncogene products. J. Biol. Chem. 269: 11590-11594.

Kazanietz, M. G., S. Wang, G. W. Milne, N. E. Lewin, H. L. Liu, and P. M. Blumberg. 1995b. Residues in the second cysteine-rich region of protein kinase C delta relevant to phorbol ester binding as revealed by site-directed mutagenesis. J. Biol. Chem. 270: 21852-21859.

Knudsen, K. A. 1990. Cell adhesion molecules in myogenesis. Curr. Opin. Cell Biol. 2: 902-906.

Kuang, S., K. Kuroda, F. Le Grand, and M. A. Rudnicki. 2007. Asymmetric self-renewal and commitment of satellite stem cells in muscle. Cell 129: 999-1010.

Laporte, J., V. Biancalana, S. M. Tanner, W. Kress, V. Schneider, C. Wallgren-Pettersson, F. Herger, A. Buj-Bello, F. Blondeau, S. Liechti-Gallati, and J. L. Mandel. 2000. Mtm1 mutations in X-linked myotubular myopathy. Hum. Mutat. 15: 393-409.

Lash, J. W., K. K. Linask, and K. M. Yamada. 1987. Synthetic peptides that mimic the adhesive recognition signal of fibronectin: Differential effects on cell-cell and cell-substratum adhesion in embryonic chick cells. Dev. Biol. 123: 411-420.

Lateva, Z. C., K. C. McGill, and M. E. Johanson. 2002. Electrophysiological evidence of adult human skeletal muscle fibres with multiple endplates and polyneuronal innervation. J. Physiol. 544: 549-565.

Lawlor, M. A., and P. Rotwein. 2000. Insulin-like growth factor-mediated muscle cell survival: Central roles for Akt and cyclin-dependent kinase inhibitor p21. Mol. Cell. Biol. 20: 8983-8995.

Lechler, T., A. Shevchenko, and R. Li. 2000. Direct involvement of yeast type i myosins in Cdc42-dependent actin polymerization. J. Cell Biol. 148: 363-373.

Legha, W., S. Gaillard, E. Gascon, P. Malapert, M. Hocine, S. Alonso, and A. Moqrich. 2010. Stac1 and stac2 genes define discrete and distinct subsets of dorsal root ganglia neurons. Gene Expr. Patterns 10: 368-375.

Linask, K. K., C. Ludwig, M. D. Han, X. Liu, G. L. Radice, and K. A. Knudsen. 1998. N-cadherin/catenin-mediated morphoregulation of somite formation. Dev. Biol. 202: 85-102.

Ma, P. C., M. A. Rould, H. Weintraub, and C. O. Pabo. 1994. Crystal structure of MyoD bHLH domain-DNA complex: Perspectives on DNA recognition and implications for transcriptional activation. Cell 77: 451-459.

Marieb, E. N., and K. Hoehn. 2010. Human anatomy and physiology. Benjamin Cummings, San Francisco, California.

Mayer, B. J., M. Hamaguchi, and H. Hanafusa. 1988. A novel viral oncogene with structural similarity to phospholipase C. Nature 332: 272-275.

McGeady, T. A. 2006. Veterinary embryology. Blackwell Pub., Oxford, Ames, Iowa.

Menko, A. S., and D. Boettiger. 1987. Occupation of the extracellular matrix receptor, integrin, is a control point for myogenic differentiation. Cell 51: 51-57.

Murray, S. A., J. L. Morgan, C. Kane, Y. Sharma, C. S. Heffner, J. Lake, and L. R. Donahue. 2010. Mouse gestation length is genetically determined. Plos One 5: e12418.

Murre, C., P. S. Mccaw, H. Vaessin, M. Caudy, L. Y. Jan, Y. N. Jan, C. V. Cabrera, J. N. Buskin, S. D. Hauschka, A. B. Lassar, H. Weintraub, and D. Baltimore. 1989.

Interactions between heterologous helix-loop-helix proteins generate complexes that bind specifically to a common DNA-sequence. Cell 58: 537-544.

Nabeshima, Y., K. Hanaoka, M. Hayasaka, E. Esumi, S. Li, and I. Nonaka. 1993. Myogenin gene disruption results in perinatal lethality because of severe muscle defect. Nature 364: 532-535.

Nakaya, Y., S. Kuroda, Y. T. Katagiri, K. Kaibuchi, and Y. Takahashi. 2004. Mesenchymal-epithelial transition during somitic segmentation is regulated by differential roles of Cdc42 and Rac1. Dev. Cell 7: 425-438.

Nguyen, J. T., M. Porter, M. Amoui, W. T. Miller, R. N. Zuckermann, and W. A. Lim. 2000. Improving SH3 domain ligand selectivity using a non-natural scaffold. Chem. Biol. 7: 463-473.

Ono, Y., T. Fujii, K. Igarashi, T. Kuno, C. Tanaka, U. Kikkawa, and Y. Nishizuka. 1989. Phorbol ester binding to protein kinase C requires a cysteine-rich zinc-finger-like sequence. Proc. Natl. Acad. Sci. USA 86: 4868-4871.

Ordahl, C. P., and N. M. Le Douarin. 1992. Two myogenic lineages within the developing somite. Development 114: 339-353.

Palmeirim, I., D. Henrique, D. Ish-Horowicz, and O. Pourquie. 1997. Avian hairy gene expression identifies a molecular clock linked to vertebrate segmentation and somitogenesis. Cell 91: 639-648.

Pas, M. F. W. T., M. E. Everts, and H. P. Haagsman. 2004. Muscle development of livestock animals : Physiology, genetics, and meat quality. CABI Pub., Wallingford, Oxfordshire, UK; Cambridge, Massachusetts.

Patapoutian, A., J. K. Yoon, J. H. Miner, S. Wang, K. Stark, and B. Wold. 1995. Disruption of the mouse MRF4 gene identifies multiple waves of myogenesis in the myotome. Development 121: 3347-3358.

Penn, B. H., D. A. Bergstrom, F. J. Dilworth, E. Bengal, and S. J. Tapscott. 2004. A MyoD-generated feed-forward circuit temporally patterns gene expression during skeletal muscle differentiation. Genes Dev. 18: 2348-2353.

Periasamy, M., D. F. Wieczorek, and B. Nadal-Ginard. 1984. Characterization of a developmentally regulated perinatal myosin heavy-chain gene expressed in skeletal muscle. J. Biol. Chem. 259: 13573-13578.

Perry, R. L., and M. A. Rudnicki. 2000. Molecular mechanisms regulating myogenic determination and differentiation. Front. Biosci. 5: D750-767.

Phillips, W. D., and M. R. Bennett. 1984. Differentiation of fiber types in wing muscles during embryonic development: Effect of neural tube removal. Dev. Biol. 106: 457-468.

Pin, C. L., A. W. Hrycyshyn, K. A. Rogers, W. J. Rushlow, and P. A. Merrifield. 2002. Embryonic and fetal rat myoblasts form different muscle fiber types in an ectopic in vivo environment. Dev. Dyn. 224: 253-266.

Pourquie, O., C. M. Fan, M. Coltey, E. Hirsinger, Y. Watanabe, C. Breant, P. Francis-West, P. Brickell, M. Tessier-Lavigne, and N. M. Le Douarin. 1996. Lateral and axial signals involved in avian somite patterning: A role for BMP4. Cell 84: 461-471.

Raska, I., K. Koberna, J. Malinsky, H. Fidlerova, and M. Masata. 2004. The nucleolus and transcription of ribosomal genes. Biol. Cell 96: 579-594.

Relaix, F., D. Rocancourt, A. Mansouri, and M. Buckingham. 2005. A Pax3/Pax7-dependent population of skeletal muscle progenitor cells. Nature 435: 948-953.

Rhodes, S. J., and S. F. Konieczny. 1989. Identification of MRF4: A new member of the muscle regulatory factor gene family. Genes Dev. 3: 2050-2061.

Robinson, R., D. Carpenter, M. A. Shaw, J. Halsall, and P. Hopkins. 2006. Mutations in ryr1 in malignant hyperthermia and central core disease. Hum. Mutat. 27: 977-989.

Ross, J. J., M. J. Duxson, and A. J. Harris. 1987. Neural determination of muscle fibre numbers in embryonic rat lumbrical muscles. Development 100: 395-409.

Rossant, J., and P. P. L. Tam. 2002. Mouse development : Patterning, morphogenesis, and organogenesis. Academic Press, San Diego, California.

Rudnicki, M. A., T. Braun, S. Hinuma, and R. Jaenisch. 1992. Inactivation of MyoD in mice leads to up-regulation of the myogenic HLH gene Myf-5 and results in apparently normal muscle development. Cell 71: 383-390.

Rudnicki, M. A., P. N. J. Schnegelsberg, R. H. Stead, T. Braun, H. H. Arnold, and R. Jaenisch. 1993. MyoD or Myf-5 is required for the formation of skeletal-muscle. Cell 75: 1351-1359.

Salminen, M., B. I. Meyer, and P. Gruss. 1998. Efficient poly a trap approach allows the capture of genes specifically active in differentiated embryonic stem cells and in mouse embryos. Dev. Dyn. 212: 326-333.

Sandri, M., and U. Carraro. 1999. Apoptosis of skeletal muscles during development and disease. Int. J. Biochem. Cell Biol. 31: 1373-1390.

Sanes, J. R., and J. W. Lichtman. 1999. Development of the vertebrate neuromuscular junction. Annu. Rev. Neurosci. 22: 389-442.

Sauer, B. 1987. Functional expression of the cre-lox site-specific recombination system in the yeast saccharomyces cerevisiae. Mol. Cell. Biol. 7: 2087-2096.

Schiaffino, S., and C. Reggiani. 2011. Fiber types in mammalian skeletal muscles. Physiol. Rev. 91: 1447-1531.

Schlessinger, J. 1994. SH2/SH3 signaling proteins. Curr. Opin. Genet. Dev. 4: 25-30.

Spiro, A. J., G. M. Shy, and N. K. Gonatas. 1966. Myotubular myopathy. Persistence of fetal muscle in an adolescent boy. Arch. Neurol. 14: 1-14.

Stahl, M. L., C. R. Ferenz, K. L. Kelleher, R. W. Kriz, and J. L. Knopf. 1988. Sequence similarity of phospholipase C with the non-catalytic region of src. Nature 332: 269-272.

Stern, H. M., A. M. Brown, and S. D. Hauschka. 1995. Myogenesis in paraxial mesoderm: Preferential induction by dorsal neural tube and by cells expressing Wnt-1. Development 121: 3675-3686.

Stockdale, F. E. 1992. Myogenic cell lineages. Dev. Biol. 154: 284-298.

Stratford, T., C. Horton, and M. Maden. 1996. Retinoic acid is required for the initiation of outgrowth in the chick limb bud. Curr. Biol. 6: 1124-1133.

Suzuki, H., J. Kawai, C. Taga, T. Yaoi, A. Hara, K. Hirose, Y. Hayashizaki, and S. Watanabe. 1996. Stac, a novel neuron-specific protein with cysteine-rich and SH3 domains. Biochem. Biophys. Res. Commun. 229: 902-909.

Takayama, H., W. J. La Rochelle, M. Anver, D. E. Bockman, and G. Merlino. 1996. Scatter factor/hepatocyte growth factor as a regulator of skeletal muscle and neural crest development. Proc. Natl. Acad. Sci. USA 93: 5866-5871.

Thompson, R. F., and G. M. Langford. 2002. Myosin superfamily evolutionary history. Anat. Rec. 268: 276-289.

Turgeon, B., and S. Meloche. 2009. Interpreting neonatal lethal phenotypes in mouse mutants: Insights into gene function and human diseases. Physiol. Rev. 89: 1-26.

Vassilopoulos, D., E. M. Lumb, and A. E. Emery. 1976. Muscle nuclear size in neuromuscular disease. J. Neurol. Neurosurg. Psychiatry 39: 159-162.

Venuti, J. M., J. H. Morris, J. L. Vivian, E. N. Olson, and W. H. Klein. 1995. Myogenin is required, for late but not early aspects of myogenesis during mouse development. J. Cell Biol. 128: 563-576.

Watson, C. M., P. A. Trainor, T. Radziewic, G. J. Pelka, S. X. Zhou, M. Parameswaran, G. A. Quinlan, M. Gordon, K. Sturm, and P. P. Tam. 2008. Application of lacZ transgenic mice to cell lineage studies. Methods Mol. Biol. 461: 149-164.

Weintraub, H. 1993. The MyoD family and myogenesis: Redundancy, networks, and thresholds. Cell 75: 1241-1244.

Wilson, S. J., and A. J. Harris. 1993. Formation of myotubes in aneural rat muscles. Dev. Biol. 156: 509-518.

Wright, W. E., D. A. Sassoon, and V. K. Lin. 1989. Myogenin, a factor regulating myogenesis, has a domain homologous to MyoD. Cell 56: 607-617.

Yagami-Hiromasa, T., T. Sato, T. Kurisaki, K. Kamijo, Y. Nabeshima, and A. Fujisawa-Sehara. 1995. A metalloprotease-disintegrin participating in myoblast fusion. Nature 377: 652-656.

Yonei-Tamura, S., T. Endo, H. Yajima, H. Ohuchi, H. Ide, and K. Tamura. 1999a. FGF7 and FGF10 directly induce the apical ectodermal ridge in chick embryos. Dev. Biol. 211: 133-143.

Yonei-Tamura, S., K. Tamura, T. Tsukui, and J. C. Izpisua Belmonte. 1999b. Spatially and temporally-restricted expression of two T-box genes during zebrafish embryogenesis. Mech. Dev. 80: 219-221.

Yoon, J. K., E. N. Olson, H. H. Arnold, and B. J. Wold. 1997. Different MRF4 knockout alleles differentially disrupt Myf-5 expression: Cis-regulatory interactions at the MRF4/Myf-5 locus. Dev. Biol. 188: 349-362.

Zhang, W., R. R. Behringer, and E. N. Olson. 1995. Inactivation of the myogenic bHLH gene MRF4 results in up-regulation of myogenin and rib anomalies. Genes Dev. 9: 1388-1399.

Zhu, X. D., and P. D. Sadowski. 1995. Cleavage-dependent ligation by the FLP recombinase. Characterization of a mutant FLP protein with an alteration in a catalytic amino acid. J. Biol. Chem. 270: 23044-23054.

Appendices

Appendix A. Gene trap mutagenesis

The mutation present in the Stac3 mice was caused by gene trap method of gene targeting mutagenesis performed by the International Knockout Mouse Consortium (IKMC) (Collins et al., 2007). This method was originally demonstrated using bacteriophage transposable elements to insert reporter genes at random locations in *E.Coli* (Casadaban and Cohen, 1979). Gene traps are randomly introduced into the genomes of embryonic stem cells by electroporation or by retroviral infection. The principle behind the gene trap method is transcriptional termination at a polyadenylation site located in an intron immediately downstream of a biomarker, typically β-glucosidase (β-gal), to allow positive selection of ES cells. Simultaneously, a neomyocin resistant sequence is transcribed to allow negative selection of ES cells. The advantage gene trapping has over other forms of mutagenesis, such as homologous recombination, is that it is a high throughput method. The fact that no target gene or homologous sequence must be identified prior to the procedure makes gene trapping an excellent method for knocking out a high number of genes in an efficient manner.

The cassette used in the specific case of Stac3 is a well characterized sequence inserted into the first intron of the coding region (Figure 6). This cassette consists of two flippase recombination enzyme (FLP) recognition target recombination sites labeled FRT, two X-over P1 (loxP) sites, a neomycin site, a β-gal site, a splice adaptor site, an internal ribosomal entry site, and two polyadenylation sites. The FRT site is used for site directed recombination in the presence of the FLP enzyme (Zhu and Sadowski, 1995). The FLP-FRT sites remove the trapping cassette rescuing the mutated phenotype. The loxP site is another site-directed recombination tool that excises the sequence between each loxP site in the presence of the Cre recombinase enzyme (Cre) (Sauer, 1987). The Cre-loxP site excises four exons and renders the transcript

nonfunctional. These two site-directed recombination inserts together comprise what is known as a conditional knockout (Bouvier and Cheng, 2009). The conditional knockout mouse allows the mutation to be rescued through the FLP/FRT recombinase mechanism and then knocked out again at the investigators discretion with the Cre/loxP recombinase mechanism. Other components of the trapping cassette primarily provide selectable markers. The neomycin site is a selectable marker used to identify the successfully transfected ES cells in the initial stage of selection. The β-gal site can be used as a marker for *in situ* procedures to identify transcription location (Salminen et al., 1998). The splice acceptor (En SA2 in this case) site links the trapping cassette in the first intron of the coding region to the first exon. This permits the β-gal to be transcriptionally regulated by the trapped promoter and use of the β-gal site as a biomarker both *in vivo* and *in vitro* for qualitative and quantitative assays (Durick et al., 1999). The internal ribosomal entry site allows for the translation of the reporter gene, β-gal, from fusion transcripts (Bonaldo et al., 1998). Finally, the polyadenylation sequence prematurely terminates the transcription of the mRNA rendering the protein nonfunctional only after the expression of the selection markers (Salminen et al., 1998).

Appendix B. Fetus collection

1. Anesthetize female by placing approximately 0.5 to 1.0 ml isoflurane (on a paper towel or Kimwipe) in a sealed cage for 45 to 60 sec followed by cervical dislocation.

2. Using scissors cut open the ventral abdominal wall exposing the uterus.

3. Separate fetuses from amniotic fluids, record weight, and collect a sample of the tail for genotyping.

4. Sever the skin of the fetuses at the sagittal plane both dorsal and ventral to allow fixative penetration and place in 10% neutral buffered formalin for 48 h.

5. After 48 h store in 70% ethanol until processed.

Appendix C. Paraffin embedding and sectioning

1. Place tissues in cassette and either in a carrousel processor or in processing station for hand processing.
    a. Dehydrate samples in 70% ethanol #1 for 1 h.
    b. Dehydrate samples in 70% ethanol #2 for 1 h.
    c. Dehydrate samples in 80% ethanol #1 for 1 h.
    d. Dehydrate samples in 80% ethanol #2 for 1 h.
    e. Dehydrate samples in 95% ethanol #1 for 1 h.
    f. Dehydrate samples in 95% ethanol #2 for 1 h.
    g. Dehydrate samples in 100% ethanol #1 for 1 h.
    h. Dehydrate samples in 100% ethanol #2 for 1 h.
    i. Clear samples in 100% xylene #1 for 1 h.
    j. Clear samples in 100% xylene #2 for 1 h.
    k. Infiltrate samples with 100% paraffin #1 for 1 h at 55 - 57˚ C.
    l. Infiltrate samples with 100% paraffin #2 for 1 h at 55 - 57˚ C.
2. Remove tissue from cassette and strategically orientate in mold and surround with paraffin by pouring paraffin heated to 55˚ C into mold.
3. Leave cool at room temperature and store.
4. Place blocks in 4˚ C one h prior to sectioning.
5. Place molds in microtome and trim at 40 μm until the specimen is nicked with blade.
6. Cut three serial sections at 6 μm thick ribbons approximately every 60 - 100 μm.
7. Place ribbons in 42˚ C water bath.
8. Carefully move a positively charged slide under the ribbons and lift out of the water bath.

9. Leave over night on slide warmer set at approximately 45˚ C and store at room temperature.

Appendix D. Deparaffinizing tissue section

1. Place slides in Coplin jar or slide carrier.
2. Using a separate container for each:
    a. Deparaffinize with 100% xylene #1 for 5 min.
    b. Deparaffinize with 100% xylene #2 for 5 min.
    c. Hydrate in 100% ethanol #1 for 1 min.
    d. Hydrate in 100% ethanol #2 for 1 min.
    e. Hydrate in 95% ethanol #1 for 2 min.
    f. Hydrate in 95% ethanol #2 for 2 min.
    g. Hydrate in 80% ethanol #1 for 2 min.
    h. Hydrate in 80% ethanol #2 for 2 min.
    i. Hydrate in 70% ethanol for 2 min.
    a. Hydrate in ddH_2O for 5 min.
2. Proceed immediately to desired histochemical procedure.

Appendix E. Hematoxylin and Eosin staining for formalin fixed paraffin embedded tissue

1. Place slides in Coplin jar of Gills Hematoxylin for 90 sec.
2. Rinse with tap water.
3. Place slides in Scott's tap water for 30 sec.
    a. Scott's tap water recipe: For working stock add 20 g $MgSO_4$ (0.2 M) with 2 g $NaHO_3$ (0.03 M) to 1 L ddH_2O
4. Rinse with tap water.
5. Place slides in 95% ethanol for 30 sec.
6. Place slides in Eosin Y alcoholic solution for 45 sec.
7. Dip slides in 70% ethanol 10 times.
8. Dip slides in 80% ethanol 10 times.
9. Dip slides in 90% ethanol 10 times.
10. Place slides in 100% ethanol for 1 min.
11. Clear slides in 100% xylene #1 for 5 min.
12. Clear slides in 100% xylene #2 for 5 min.
13. Mount cover slip with Protocol® SecureMount™ mounting medium diluted with xylene without allowing the slide to dry.

Appendix F. Hematoxylin and Eosin staining frozen tissue

1. Place sections from freezer immediately into 10% neutral buffered formalin for 5 min.

2. Wash in PBS for 5 min.
    a. Repeat step 1.
    b. Repeat step 1.

1. Place slides in Coplin jar of Gills Hematoxylin for 90 sec.

2. Rinse with tap water.

3. Place slides in Scott's tap water for 30 sec.

4. Rinse with tap water.

5. Place slides in 95% ethanol for 30 sec.

6. Place slides in Eosin Y alcoholic solution for 45 sec.

7. Dip slides in 70% ethanol 10 times.

8. Dip slides in 80% ethanol 10 times.

9. Dip slides in 90% ethanol 10 times.

10. Place slides in 100% ethanol for 1 min.

11. Clear slides in 100% xylene #1 for 5 min.

12. Clear slides in 100% xylene #2 for 5 min.

13. Mount cover slip with Protocol® SecureMount™ mounting medium diluted with xylene without allowing the slide to dry.

Appendix G. Antigen retrieval

1. Heat citrate buffer to boiling in a microwave then place on hotplate and stabilize temperature at 95 - 100˚ C.

    a. Citrate buffer recipe: For working stock add 13.5 ml 0.1 M citrate acid monohydrate with 61.5 ml 0.1 M sodium citrate dihydrate and bring to 750 ml with ddH_2O.

2. Place slides in heated citrate buffer for 30 min.

3. Remove from heat source and allow citrate buffer and slides to cool for 20 min at room temperature.

4. Wash in PBST (PBS + 0.05% Tween-20) #1 for 2 min.

5. Wash in PBST #2 for 2 min.

6. Proceed to desired primary antibody protocol.

Appendix H. Immunohistochemistry

1. Block slides with 5% goat serum in PBS (or serum from host of selected secondary antibody if available) at room temperature for 1 h in covered container.

2. Add primary antibody directly on the specimen and incubate overnight at 4˚ C in a covered dish.

3. Specific antibody specifications:
    a. MF20 IgG2b (Myosin heavy chain): 1:200.
    b. F5D IgG1 (Myogenin): 1:100.
    c. M-318 IgG (MyoD): 1:100.

4. Wash in PBS #1 for 5 min at room temperature.
    a. Wash in PBS #2 for 5 min at room temperature.
    b. Wash in PBS #3 for 5 min at room temperature.

5. Add secondary antibody or multiple for double labeling, plus DAPI counter stain directly on the specimen and incubate for 1 h at room temperature.

6. Specific antibody specifications:
    a. Goat anti-mouse IgG DyLight® 594 Conjugated (Product 35511): 1:200.
    b. Wheat Germ Agglutinin Alexa Fluor® 488 conjugate (Product W11261): 1:400.
    c. DAPI: 1:1000.

7. Wash in PBS #1 for 5 min at room temperature.
    a. Wash in PBS #2 for 5 min at room temperature.
    b. Wash in PBS #3 for 5 min at room temperature.

8. Place one drop of Sudan Black directly on specimen for 1 min.
    a. Filtered 0.1% Sudan Black B in 70% ethanol.

9. Wash in PBS for min.

10. Dry back of slide with Kimwipe and remove excess PBS from top of slide with vacuum.

11. Mount with Prolong® Gold antifade reagent mounting medium.

12. Add thin streak of nail polish to perimeter of cover slide to prevent drying of the mounting medium.